INVESTIGATION OF THE SILICON NITRIDE COATING THICKNESS ON SILICON WAFER SUBSTRATES FOR ENHANCED SENSITIVITY IN DRIED NANO-DROPLET ANALYSIS BY LASER INDUCED BREAKDOWN SPECTROSCOPY

A Thesis Submitted to
the Graduate School of Engineering and Sciences of
İzmir Institute of Technology
in Partial Fulfillment of the Requirements for the Degree of

MASTER OF SCIENCE

in Chemistry

by

Dilara DURKAN KAPLAN

July 2021

İZMİR

ACKNOWLEDGMENTS

I would like to thank everyone who has helped and contributed to the development of my thesis so far.

First of all, I would like to thank my very esteemed advisor, Prof. Dr. Şerife YALÇIN, who shared her valuable information with me during the realization of this study and I will never forget the importance of every word she used. I am grateful to my advisor for devoting her time to me and my studies, and for her approval to work with her first and foremost.

I would like to thank all the committee members individually for giving their precious time to my study.

Also, I would like to thank to my laboratory mate Özge TETİK KARABIYIK for her support, her great friendship and all enjoyable time we had together.

I would like to express my most special thanks to my dear family; my mother Dilek DURKAN and my father Rahmi DURKAN for bringing me to this day and for being by my side under all circumstances. I am grateful for all their effort and endless support they have given me throughout my life. I would also like to thank my life partner Ali KAPLAN, who has been my biggest support in every moment of my life, for all his care and attention towards me.

I would like to thank TÜBİTAK for financial support (119F068).

ABSTRACT

INVESTIGATION OF THE SILICON NITRIDE COATING THICKNESS ON SILICON WAFER SUBSTRATES FOR ENHANCED SENSITIVITY IN DRIED NANO-DROPLET ANALYSIS BY LASER INDUCED BREAKDOWN SPECTROSCOPY

Laser Induced Breakdown Spectroscopy (LIBS) is an atomic emission spectroscopic technique that uses laser beam to generate plasma for detection. Also, LIBS is a fast and non-destructive methodology with the advantage of no sample preparation requirement and easy usage.

Surface Enhanced LIBS (SENLIBS) is recently developed version of the LIBS technique that uses some kinds of surface materials for supporting liquids and for the enhancement of LIBS signal intensity. It has been previously shown that silicon nitride coated silicon wafer substrates have some properties to enhance LIBS signal of several metal solutions by dried-droplet analysis methodology. Within the scope of this thesis study, silicon wafers coated with silicon nitride of several thicknesses were utilized for investigating the effect of coating thickness on sensitivity of the LIBS technique for liquids analysis.

Heavy metals above a certain concentration have a significant negative impact on the environment and human health. In this context, the chromium, copper and lead metal liquid samples was loaded on 75 nm, 300 nm, 450 nm and 1000 nm silicon nitride coated wafers and dried, then analyzed by LIBS. As a result of this study, it was seen that the 1000 nm coating increased the LIBS signal intensity at the highest degree. The LOD value of the chromium element was improved as 0.56 pg, the lead element as 0.7 pg, and the copper element as 0.42 pg with 1000 nm Si_3N_4 coated wafers.

ÖZET

LAZER OLUŞTURMALI PLAZMA SPEKTROSKOPİSİ İLE KURUTULMUŞ NANO-DAMLACIK ANALİZİNDE ARTTIRILMIŞ HASSASİYET İÇİN SİLİSYUM GOFRET ALTTAŞLAR ÜZERİNDEKİ SİLİSYUM NİTRÜR KAPLAMA KALINLIĞININ ARAŞTIRILMASI

Lazer Oluşturmalı Plazma Spektroskopisi (LIBS), elemental analiz için plazma oluşturmak üzere lazer ışını kullanan atomik emisyon spektroskopik bir tekniktir. Ayrıca LIBS, numune hazırlama gereksinimi olmaması ve kolay kullanım avantajı ile hızlı ve tahribatsız bir metodolojidir.

Yüzeyde güçlendirilmiş LIBS (SENLIBS), sıvıları desteklemek ve LIBS sinyal yoğunluğunu arttırmak için bazı yüzey malzemeleri kullanan LIBS tekniğinin yakın zamanda geliştirilmiş versiyonudur. Silisyum nitrür kaplı silikon gofret substratlarının, kurutulmuş damlacık analizi metodolojisi ile birkaç metal solüsyonunun LIBS sinyalini geliştirmek için bazı özelliklere sahip olduğu daha önce gösterilmişti. Bu tez çalışması kapsamında, sıvıların analizi için LIBS tekniğinin duyarlılığına kaplama kalınlığının etkisini araştırmak için çeşitli kalınlıklarda silikon nitrür ile kaplanmış silikon gofretler kullanılmıştır.

Belirli bir konsantrasyonun üzerindeki ağır metaller, çevre ve insan sağlığı üzerinde önemli derecede olumsuz etkiye sahiptir. Bu kapsamda krom, bakır ve kurşun metalleri sıvı numuneleri 75 nm, 300 nm, 450 nm ve 1000 nm silikon nitrür kaplı tabakalara yüklenmiş ve kurutulduktan sonra LIBS ile analiz edilmiştir. Bu çalışma sonucunda 1000 nm kaplamanın LIBS sinyal yoğunluğunu en yüksek derecede artırdığı görülmüştür. 1000 nm Si_3N_4 kaplı wafer ile krom için tayin limiti (LOD) değeri 0.56 pg, kurşun için 0.7 pg ve bakır için 0.42 pg olarak iyileştirildi.

TABLE OF CONTENTS

LIST OF FIGURES……vii

LIST OF TABLES……...xi

LIST OF SYMBOLS AND ABBREVIATIONS…….……...xii

CHAPTER 1: INTRODUCTION……...…..…1

1.1. Laser Induced Breakdown Spectroscopy (LIBS)…….…..…..1

1.1.1. Principles of the LIBS……..……..……1

1.1.2. Physical Plasma Parameters, Electron Temperature, Electron Density……...3

1.1.3. Instrumentation……...5

1.1.4 Advantages and Disadvantages of LIBS…….…..…..8

1.2. Liquid Analysis by LIBS……..…….…….……..9

1.3. Dried-Droplet Analysis by LIBS…….……..….12

1.4. Elements Studied: Chromium, Copper, Lead…….……...13

1.5. Aim of the Study……..……..…….16

CHAPTER 2: SURFACE ENHANCED LIBS (SENLIBS)..…….……17

2.1. Theory of the SENLIBS.…….…...…..17

2.2. Silicon Nitride (Si_3N_4) Coating…….……...….……...20

2.2.1. Silicon Nitride; Production, Properties and Applications….....20

2.3. Light-Matter Interaction.……...…….…….…….21

2.3.1. Reflection…….……..……..……..…21

2.3.2. Refraction…..……..…….…….…22

2.3.3. Anti-Reflection Coating (ARC)……..…….……...……..23

CHAPTER 3: EXPERIMENTAL STUDY…….…….……...25

3.1. Experimental LIBS Set-Up……..……..……...25

3.2. Substrates and Chemicals…..……...……26

3.2.1. Silicon Nitride Coated Wafers and Apparatus…….……..26
3.2.2. Chemicals and Standart Solutions…….……28
3.3. Dry-Droplet Analysis…….……..…….30
3.4. Optimization Studies of LIBS Set-Up……...……..……32

CHAPTER 4: RESULT AND DISCUSSION……...…….…….34
4.1. Reflectance Measurements…...……...…….34
4.2. Optimization of the Instrumental LIBS Parameters for Heavy Metal..36
4.2.1. Optimization of Chromium – Cr(I) signal……...…….…..36
4.2.2. Optimization of Copper – Cu(I) signal……...…38
4.2.3. Optimization of Lead – Pb(I) signal……...…40
4.3. Representative LIBS Spectra…….....……..42
4.4. Variation of signal intensity with Si_3N_4 coating thickness…...……44
4.5. Calibration Studies...……..…..……..47
4.6. Analytical Performance of the substrates…….....51
4.6.1. Certified Reference Materials, CRM, and Real Waters Analysis..52
4.6.2. Recovery studies from spiking experiments...…….....57

CHAPTER 5: CONCLUSION…….....…..63

REFERENCES

LIST OF FIGURES

Figure **Page**

Figure 1.1. Formed plasma after striking laser beam to the sample……....2

Figure 1.2. Representative LIBS spectrum……2

Figure 1.3. General LIBS Setup…….5

Figure 1.4. Laser path through the setup……6

Figure 1.5. Schematic draw of laser…….…..6

Figure 1.6. a) Absorption, b) Spontaneous Emission……..…7

Figure 1.7. Stimulated Emission……7

Figure 1.8. Picture of CCD……8

Figure 1.9. Setup for hydride generation technique…….11

Figure 1.10. SEM images of a) Si+SiO2 surface, b) 500 nL dried droplet of 1 mg/L copper solution, c) a crater after laser ablation of drying droplet by a 200 mJ single laser pulse, d) 16 sequential sampling in a single droplet area with tightly focused laser pulses and, e) the enlarged view of one of the craters given in (d)…….…….12

Figure 1.11. Lead…….14

Figure 1.12. Copper…….14

Figure 1.13. Chromium……15

Figure 2.14. Reflection of the beam…….....22

Figure 2.15. Diffuse reflection (left), specular reflection (right)…….….22

Figure 2.16. Refraction of the beam……..…23

Figure 3.17. Block Diagram of the Experimental LIBS Set-up……...26

Figure 3.18. a) 75 nm b)300 nm c) 450 nm d) 1000 nm Si_3N_4 coated silicon wafers.…27

Figure **Page**

Figure 3.19. Apparatus used to fix different thicknesses at the same point……..…27

Figure 3.20. Heavy metal solutions…….…….……28

Figure 3.21. Multielement solutions……..……..29

Figure 3.22. SLRS4 Riverine water solution……29

Figure 3.23. Dry Droplet Analysis……...30

Figure 3.24. 75 nm (blue), 300 nm (pink), 450 nm (green) , 1000 nm (grey) silicon nitride coated wafers , while the drops are loaded (left), after dry-droplets are analysed by LIBS (right)……....31

Figure 3.25. SEM image of 500 nl dried droplet of the heavy metal sample……..…..31

Figure 3.26. SEM image of the dried droplet sample after analyzed with LIBS……..….32

Figure 4.27. Si_3N_4 (75 nm, 300 nm, 450 nm, 1000 nm) reflectance measurement spectrum in any thickness from 200 nm to 800 nm……..…..34

Figure 4.28. 500 nL 100 ppb Chromium solutions were dropped onto 300 nm Si_3N_4 coated wafers, and optimized about delay time, gate width and laser energy by LIBS…….....37

Figure 4.29. Grotrian diagram of Cr(I)…….38

Figure 4.30. 500 nL 100 ppb Copper solutions were dropped onto 300 nm Si_3N_4 coated wafers, and optimized about delay time, gate width and laser energy by LIBS….……..….39

Figure 4.31. Grotrian diagram of Cu(I)……40

Figure 4.32. 500 nL 100 ppb Lead solutions were dropped onto 300 nm Si_3N_4 coated wafers, and optimized about delay time, gate width and laser energy by LIBS……...….41

Figure 4.33. Grotrian diagram of Pb(I)……..…..42

Figure **Page**

Figure 4.34. Descriptive LIBS spectra obtained from plasma generated by laser pulses of 130 mJ energy followed by drying of 500 nL Cr solution at a concentration of 50 microgram loaded onto a) 300 nm, b) 75 nm, c) 450 nm and d) 1000 nm Si_3N_4 coated surface……..43

Figure 4.35. Descriptive LIBS spectra obtained from plasma generated by laser pulses of 130 mJ energy following drying of 500 nL Cu solution at a concentration of 50 microgram / L loaded onto a) 300 nm, b) 75 nm, c) 450 nm and d) 1000 nm Si_3N_4 coated surfaces……..43

Figure 4.36. Descriptive LIBS spectra obtained from plasma generated by laser pulses of 130 mJ energy following drying of 500 nL Pb solution at a concentration of 50 microgram / L loaded onto a) 300 nm, b) 75 nm, c) 450 nm and d) 1000 nm Si_3N_4 coated surfaces……44

Figure 4.37. The variation of signal intensities at different silicon nitride coating thicknesses in dry drop analysis of Pb, Cu and Cr solutions……..…45

Figure 4.38. Plasma temperature study……46

Figure 4.39. Cr (I) (428.9 nm) LIBS signal obtained from Cr solutions in the concentration range of 1ppb - 100 ppb on 75nm, 300nm, 450nm, 1000nm Si_3N_4 coated wafer layers……..48

Figure 4.40. Cu (I) (324.7 nm) LIBS signal obtained from Cu solutions in the concentration range of 1ppb - 100 ppb on 75nm, 300nm, 450nm, 1000nm Si_3N_4 coated wafer layers…….……..…..…48

Figure 4.41. Pb (I) (405.8 nm) LIBS signal obtained from Pb solutions in the concentration range of 1ppb - 100 ppb on 75nm, 300nm, 450nm, 1000nm Si_3N_4 coated wafer layers……..….49

Figure 4.42. 0.25 ppb Cr calibration curve with 1000 nm coated Si_3N_4, LIBS spectra for 0.25 ppb Cr with 75 nm, 450 nm and 1000 nm Si_3N_4 coated wafers……..…….51

Figure **Page**

Figure 4.43. LIBS analysis of DWS solution under the conditions optimized for Cr - Sample is diluted to contain 30ppb Cr…….……53

Figure 4.44. LIBS analysis of ERM solution under the conditions optimized for Cu - Sample is diluted to contain 50ppb Cu……..…….54

Figure 4.45. LIBS analysis of ICP-PES solution under the conditions optimized for Lead - Sample diluted to 50ppb Pb……...……55

Figure 4.46. Relative signal intensity of the elements Pb, Cu and Cr on 300 nm and 1000 nm Si_3N_4 coated wafers for ICP-PES, ERM and DWS water sample...57

Figure 4.47. A region of the LIBS spectrum from the analysis of SLRS-4 river water sample……..…58

Figure 4.48. The calibration graph for 70, 50, 30 and 10 ppb Cr spiked river water samples……. 58

Figure 4.49. A region of the LIBS spectrum from the analysis of OZSU water sample…59

Figure 4.50. The calibration graph for 70, 50, 30 and 15 ppb Pb spiked OZSU water samples……..……60

Figure 4.51. A region of the LIBS spectrum for Cu, from the analysis of OZSU water sample……..……..61

Figure 4.52. The calibration graph for 70, 50, 30 and 10 ppb Cu spiked OZSU water samples……..……61

LIST OF TABLES

Table **Page**

Table 4.1. Reflectivity data for the substrates with different coating thicknesses within the spectral range of interest around 532 nm……35

Table 4.2. Optimum parameters for Cu(I), Cr(I) and Pb(I)…….……..…42

Table 4.3. Ratio of signal intensities of heavy metal elements (100 ppb) with wafers of different thickness to signal intensity with 300 nm silicon nitride coated wafer……45

Table 4.4 Plasma temperature and electron density values for copper……..47

Table 4.5. Detection limits obtained from the calibration curves of copper, chromium and lead elements on 75 nm, 300 nm, 450 nm and 1000 nm Si_3N_4 coated wafer by dry drop LIBS method……..……49

Table 4.6. Some detection limits from the literature for chromium, copper and lead by LIBS…….……..…50

Table 4.7. Signal / noise ratios with 10 ppb concentration of heavy metal elements…….51

Table 4.8. Performance characteristics of 1000 nm nitride coated wafer for dry-droplet LIBS analysis……..……..…56

Table 4.9. Percent Recovery values obtained from Cr Spiking study…….…….59

Table 4.10. Percent Recovery values obtained from Pb spiking study…….60

Table 4.11. Percent Recovery values obtained from Cu spiking study……..…..62

LIST OF SYMBOLS AND ABBREVIATIONS

LIBS	Laser-Induced Breakdown Spectroscopy
LIPS	Laser-Induced Plasma Spectroscopy
LAS	Laser Ablation Spectroscopy
n_i	ratio of the ionic particles
n_n	ratio of the non-ionic particles
α	degree of ionization
N_k	upper level atom population
N_i	ground level atom population
g	statistical weight
E_k	energy of upper level
k	Boltzmann constant
T	temperature
h	Planck constant
c	speed of light
A_{ki}	transition probability
λ	wavelength
I	intensity
FWHM	full width half maximum
LTE	local thermal equilibrium
Nd:YAG	Neodymium-Yttrium Aluminum Garnet
CCD	charged coupled detector
ICDD	Intensified Charge Coupled Detector
nm	nanometer
MHz	megahertz
Cr	Chromium
Cu	Copper
Pb	Lead
mg	milligram
µg	microgram

ppm	parts per million
ppb	parts per billion
SENLIBS	Surface-Enhanced Laser-Induced Breakdown Spectroscopy
SEM	Scanning Electron Microscope
EPA	Environmental Protection Agency
WHO	World Health Organization
LOD	limit of detection
S/N	Signal-to-Noise-Ratio
pg	picogram
ns	nanosecond
mj	milli-Joule
mL	milliliter
nL	nanoliter
CVD	chemical vapour deposition
PECVD	plasma enhanced chemical vapour deposition
t_d	Delay Time
t_g	Gate Time
Si_3N_4	Silicon Nitride
SiO_2	Silicon Oxide
c-Si	crystalline silicon
n	refractive index
ARC	anti reflection coating
d	thickness
DWS	Drinking Water Metal Solution
HPS	High Purity Standars
ERM	European Reference Material
ICP-PES (TMS)	Inductively Coupled Plasma-Plasme Emission Solution (Trace Metal Solution)
SI	Signal Intensity

CHAPTER 1

INTRODUCTION

1.1 . Laser Induced Breakdown Spectroscopy (LIBS)

Laser Induced Breakdown Spectroscopy, LIBS, also named as Laser Induced Plasma Spectroscopy (LIPS), and Laser Ablation Spectroscopy (LAS), is an elemental analysis technique that is under vigorous investigation since 1960s (Cremers D. and Radziemski, 2006). It is an advantageous, fast and useful technique that combines the fundamental principles of plasma physics with chemical analysis. LIBS is an atomic emission spectroscopic technique that uses highly energetic laser pulses for vaporization, atomization and excitation of the sample for plasma formation (Radziemski, 1989). Spectral emission from the luminous plasma is analyzed by a spectrograph for qualitative and quantitative detection.

1.1.1. Principle of the LIBS

In Laser Induced Breakdown Spectroscopy, a laser beam coming from a pulsed laser source, is directed with reflective mirrors and focussed onto the sample using focussing lenses. When energetic laser beam strikes onto the sample, and exceeds a certain threshold, an optical breakdown occurs, sample gets excited, ionized and vaporized into a hot vapour called “plasma”. Plasma has atoms in the neutral and ionic state, high number of electrons and molecules from the recombinations of the ionic species.

Immediately after plasma formation, when the laser is off, the plasma starts to decay, excited electrons and ions emit back to the ground state and cools. In this way, each element radiates at its own characteristic wavelength. A pictorial representation of

a luminous plasma is given in Fig.1.1. Spectral resolution of this plasma emission with a suitable spectrograph provides qualitative and quantitative information about the sample analyzed.

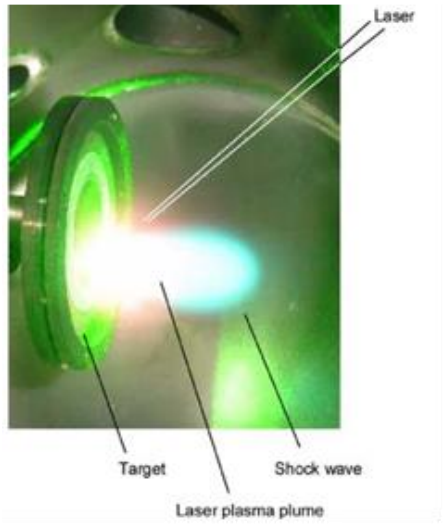

Figure 1.1. Pictorial representation of the plasma after laser beam strikes on to the sample.

A typical LIBS spectrum of a sample containing several elements is given in Figure 1.2. The peak positions provide qualitative information about the metals present, and magnitude of the peaks in terms of signal strength gives relative amounts of the species, quantitatively. The observed signal strength is directly related with the amount ablated. Higher the sample amount ablated, higher the signal strength of analyte species.

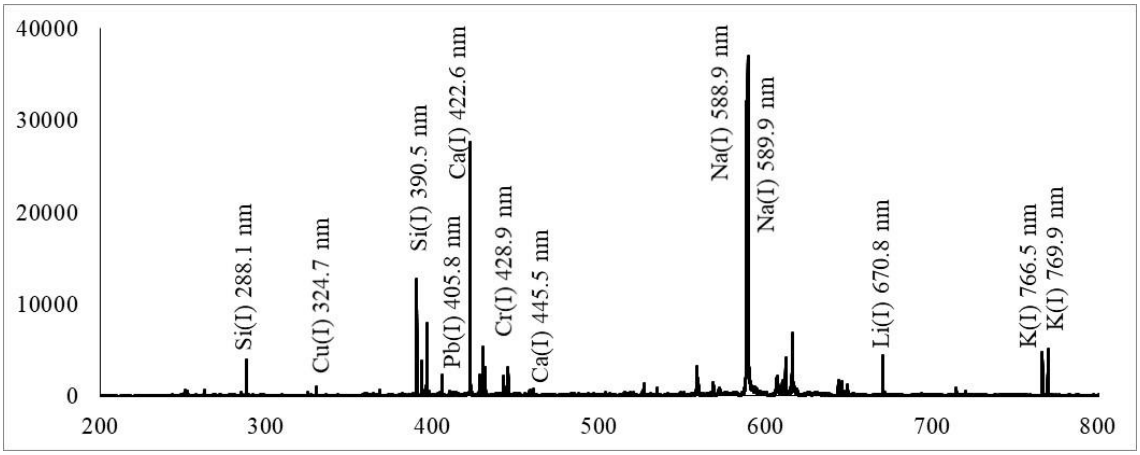

Figure 1.2. Representative LIBS spectrum

1.1.2. Physical Plasma Parameters, Electron Temperature, Electron Density

Plasma is a cloud of ionized gas containing positive and negative particles and has an electrically neutral environment, means that the overall charge of the plasma is about zero. Although plasma is totally neutral, it is electrically and heat conductive since it contains charged particles.

In addition, degree of ionization, electron temperature and the plasma electron density are some of the physical plasma parameters. Plasma parameters report the quality of the plasma. Parameters such as plasma temperature, electron density are interdependent. Laser induced plasma has high electron density on the orders of 10^{17} - 10^{18} electrons/cm^3 and high temperature of about tens of thousands Kelvin.

Plasma must be able to sustain sufficient ionization on a basis and must be hot enough for this ionization to continue. As the first parameter, *the degree of ionization* is obtained by the ratio of ionic particles (n_i) to totaly ionic and nonionic particles ($n_i + n_n$). The degree of ionization is indicated by α.

$$\alpha = \frac{n_i}{n_i + n_n} \qquad (1.1)$$

LIBS plasmas are weakly ionized plasmas. Positive and negative particles in the plasma when viewed in total are neutral or close to neutral.

Plasma temperature is generally calculated from the line intensities of ions to neutral ones, and neutral to neutral ones, mostly for the same element. For this calculation, Boltzmann and Saha-Boltzmann equation is used. Boltzmann equation is the oldest graphical approach based on the use of multiple atomic emission lines of an element (Griem, 1964).

$$\mathrm{N_k} = \mathrm{N_i}\left(\frac{g_k}{g_i}\right)\mathrm{e}^{\left(\frac{-\mathrm{E_k}}{\mathrm{kT}}\right)} \quad (1.2)$$

N refers the atom population, and subscribes as k, i refers the state of the species. ‘g’ values are the statistical weight, E_k is the energy of upper level, k is the Boltzmann constant and T is the temperature. When the line intensity equation is arranged and inserted into the Boltzmann equation, a new form of the equation is transformed into,

$$I_{ki} = \frac{hcN_i g_k A_{ki}}{4\pi\lambda z} e^{\left(\frac{-E_k}{kT}\right)} \qquad (1.3)$$

For this equation, h is the Planck constant, c is the velocity of light, A_{ki} is the transition probability and the λ is the wavelength. To perform the iteration this equations, this line equation is rearranged by taking logarithm,

$$\ln\left(\frac{I\lambda}{gA}\right) = \frac{-Ek}{kT} - \ln\left(\frac{4\pi Z}{hcN_0}\right) \quad (1.4)$$

For the plasma temperature calculation, the wavelengths seen in the LIBS spectrum of an element and the signal intensities obtained at this wavelength are used. Energy, E_k (in eV), degenarcy, g, and transition probability, A, values corresponding to each wavelength, λ, are used with a graphical approach. A line drawn for $\ln I\lambda/gA$ versus the E_k values enables temperature calculation from the slope of this line. This slope is equal to the -1/kT. Thus, plasma temperature is calculated.

The plasma electron density is an important plasma parameter needs to be known to characterize the plasma and its spectral features. It is calculated by using FWHM of Stark Broedened spectral lines. As a result of the derived and adjusted equations, the electron density is obtained by looking at certain constants using the following formula.

$$\Delta\lambda_{FWHM} = 2\omega\left(\frac{N_e}{10^{16}}\right) \quad (1.5)$$

Where $\Delta\lambda_{FWHM}$ is the line at full width half maximum, w is electron impact parameter, Ne is the electron density of the plasma.

Local Thermal Equilibrium, LTE, is the state in which all the atoms, electrons, ions in a plasma volume have the same temperature, or the velocity of the particles are equal when these particles are at the same temperature. Although plasma can never provide thermal equilibrium fully, it is possible only locally.

In order a plasma to be considered in local thermodynamic equation, the criterion

$$Ne > 1.6x10^{12} . \Delta E^3 . \sqrt{Te} \quad (1.6)$$

should be satisfied

where; Ne is the number of electron density in cm^{-3}, T is the plasma temperature in K and ΔE in eV is the highest energy difference between possible lower and upper energy levels.

The conditions of the plasma produced by intense laser pulses depends on some other parameters. The gas contained in the environment, the laser spot size, the laser wavelength and the material of the sample used are some of them.

1.1.3. Instrumentation

The experimental set-up of the Laser Induced Breakdown Spectroscopy consisted of; a laser source, optical equipments and a detection system. Figure 1.3 shows the general experimental LIBS ınstrumentation. Neodymium-doped Yttrium Aluminum Garnet (Nd:YAG) laser is the most widely laser source in LIBS experiments. The light beam from the Nd:YAG source in near-infrared region at 1064 nm and its second harmonic at 532 nm could be used. Highly energetic laser pulse from a Q-switched Nd:YAG laser source is directed by reflective mirrors and focused by focussing lenses on the sample. When the laser beam strikes on to the sample, the sample is vaporized, atomized, ionized and excited and hence a luminous plasma is formed. The light emitted from the plasma is collected by suitable optics. A fiber optic cable is used to carry plasma emission onto the entrance slit of an echelle spectrograph, and analyzed with a time resolved CCD detector.

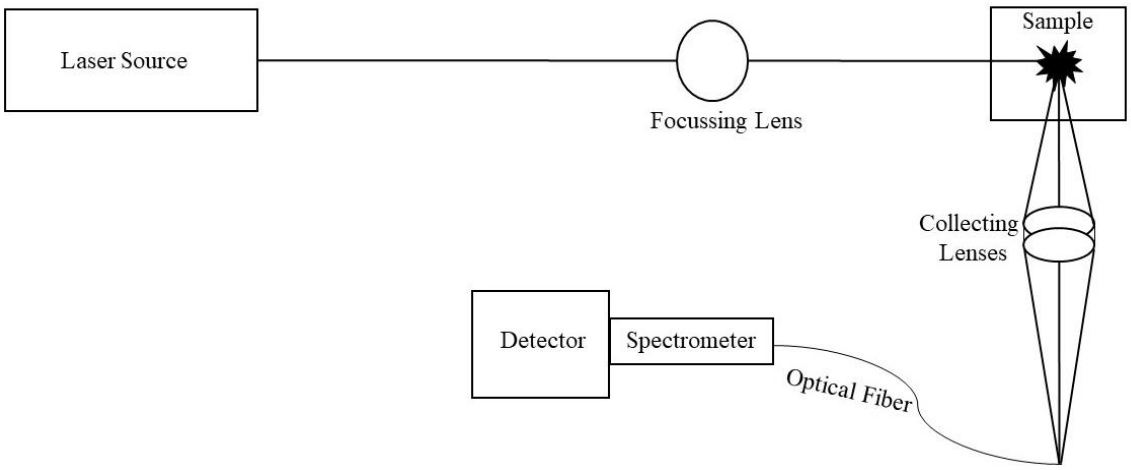

Figure 1.3. General LIBS Setup

The experimental set-up used in this study is given in detail in Chapter 3.

Lasers: A laser is a device that emits light through a process of optical amplification based on the stimulated emission of electromagnetic radiation. There needs to be three distinct things to make a laser; *active medium*, *pumping source* and *optical resonator* (Figure 1.5). Active medium contains lasing material (solid, gas, or liquid), that can be certain crystals, glasses, gases, semiconductors and dye solutions. Also, this active medium is known as amplifying or gain medium. These lasing materials in the gain medium are excited by the pumping source, to produce population inversion. In the gain medium spontaneous and stimulated emission of the photons occur. This pumping source can be either an electrical current, xenon flash lamp or another laser light.

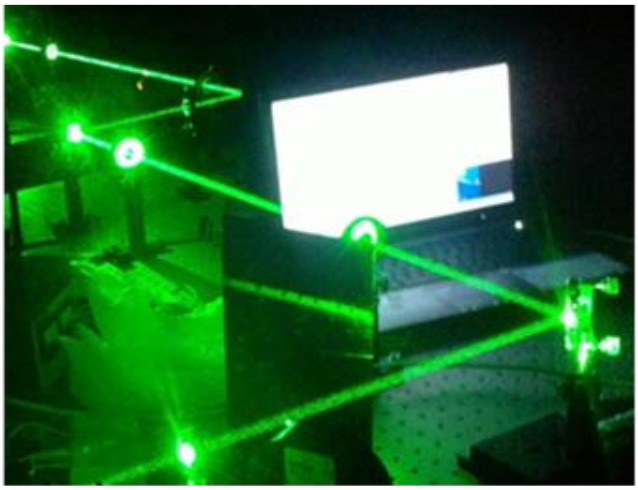

Figure 1.4. Laser path through the setup

During analysis with LIBS, the laser beam exiting the laser source and sent onto the sample material with mirrors and lenses can be seen in Figure 1.4.

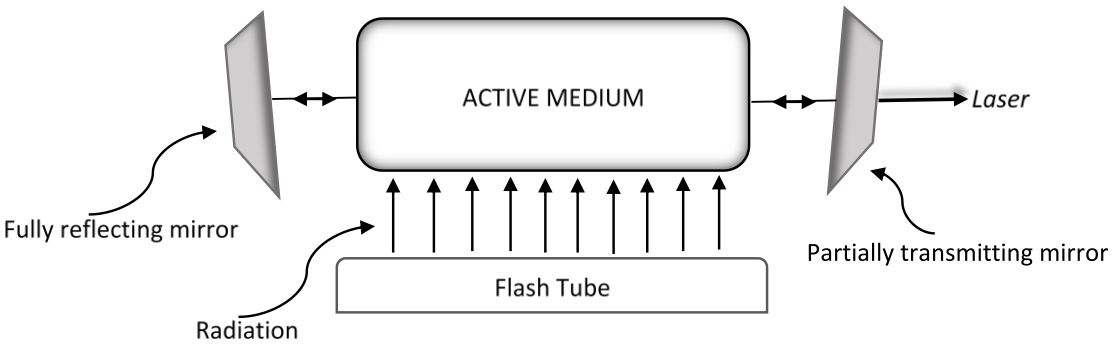

Figure 1.5. Schematic draw of laser

Absorption is the electronic or molecular transition from the lower state to the upper energy state (Figure 1.6a). These atoms that take place on the upper energy state, return to the lower state, and this return occurs without any external energy. Then, a photon is emitted as quantized amount of energy. This emission process 'without any external energy' is called as *spontaneous emission* (Figure 1.6b).

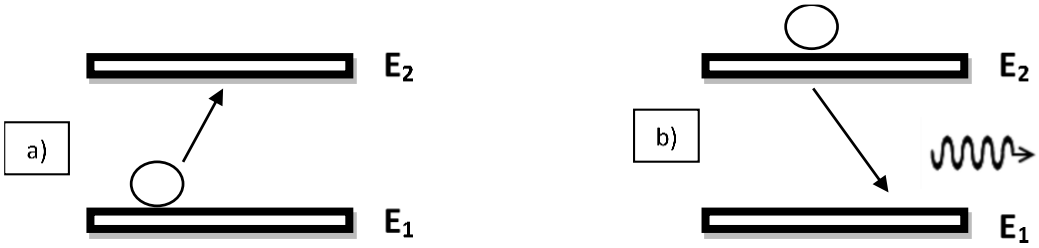

Figure 1.6. a) Absorption, b) Spontaneous Emission

However, if the atom of the excited state encounters another photon while returning to the lower energy state, it produces additional photon with the same energy, frequency, phase. This another photon behaves like external energy so this process is called as *stimulated emission* (Figure 1.7).

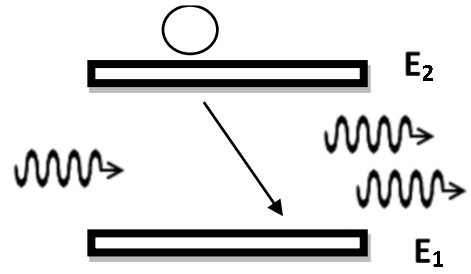

Figure 1.7. Stimulated Emission

The third component of a laser system is optical resonator, which is comprised of two parallel mirrors located to the ends of a gain medium, one is fully another is partially reflective. The light inside the cavity is reflected back and fort hundreds of times before leaving the cavity to produce laser beam.

Detector: Charged-Coupled Device, CCD, is the most widely used detector in LIBS research. CCD discovery appeared in 1969 by Willard Boyle and George Smith and has been used since then to take various images of space exploration (Charge-coupled device, Wikipedia, The Free Encyclopedia).

A CCD consists of photo diodes arranged in array on a layer (Figure 1.8). The first thing CCDs usually do is capture photons from the light source. The light coming there is converted into electrical voltage. The captured photons create photoelectrons by photon matter interaction (photoelectric event). Electrons are collected in cells (pixels) and converted into digital units by charge transfer mechanism. The next process is to the process of storing it together with its coordinates, that is Readout (Hainaut and Oliver R., 2006).

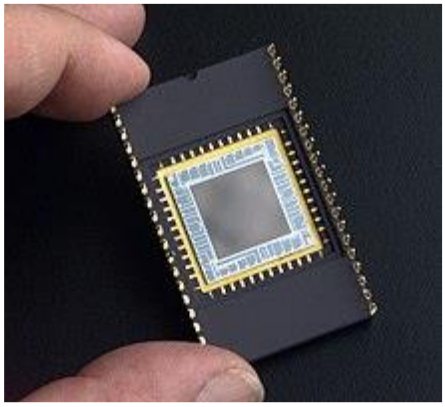

Figure 1.8. Picture of CCD

(Charge-coupled device, Wikipedia, The Free Encyclopedia)

This LIBS system has an intensified charged coupled device (ICCD) for elemental analysis. Intensifier coupled charged-coupled devices consists of the combination of the intensifier and the charged-coupled detector. Intensifier has the electron multiplying component. For this reason, it is very suitable for single photon applications or low light use. Also, ICCD is optimal for the less than nanosecond exposure time applications, like LIBS.

1.1.4. Advantages & Disadvantages of LIBS

Laser Induced Breakdown Spectroscopy is a type of atomic emission analysis technique and LIBS is a very advantageous technique compared to other similar analytical techniques.

LIBS is *a multi-element* analysis technique in which simultaneous detection of all elements in the periodic table. The technique can be applied to the analysis of solid, liquid, and gaseous samples and therefore finds large-scale application area. Also, LIBS requires *little or no sample preparation steps* that eliminates undesired contamination. Hard materials like solids can be analyzed by no sample preparation. This property provides a great advantage over other similar techniques. For LIBS analysis, laser beam is focussed onto tiny spot of microns size and therefore very small amount of sample is removed from the surface. Therefore, LIBS can be considered as nearly *non-destructive* process. As another advantage, instead of surface analysis, some parameters can be changed and *depth resolution analysis* can be done with this technique. In-situ analysis by LIBS can be performed for direct analysis. Shortly, LIBS is one of the spectroscopic technique that enables simple, rapid, accurate and low-cost analysis.
Besides all these advantages, LIBS technique also has some disadvantages. LIBS realize the analysis process by striking the laser beam to the sample surface. However, this surface can be different from bulk sample. So, this situation leads to the incorrect spectral result. Due to the fluctuations of laser energy, shot to shot reproducibility may change. This issue can also lead to false results. Detection limits obtained for most of the elements are in low ppb. So, in order to increase the analytical capability of the technique, sensitive methodologies are required.

1.2. Liquid Analysis by LIBS

Although solid analysis by LIBS is pretty straightforward process and less problematic, direct liquid analysis by LIBS has some experimental challenges.

When the laser beam strikes on to the liquid sample bubble formation, shock wave formation and splashing occurs. Therefore, poor signal quality, reduced plasma emission and low limit of detection are observed. Those worsen the analytical figures of merits of the technique.

In order to overcome these disadvantages, some researchers are using common atomic spectroscopic sample introduction techniques. *Aerosol Formation* is one of them. An aerosol is formed by dispersing liquid or solid particles in a gas environment. These

liquid or solid particles spread in the gas environment in sizes smaller than 10 microns. The aerosol method allows a liquid to be sprayed in gaseous form and under pressure (Colbeck I., Lazaridis M., 2014).

In literature, Hahn and Lunden worked on aerosol formation of calcium and magnesium solutions and detection with LIBS (Hahn D. and Lunden M., 2000). They measured the aerosol particles about 175 nm in diameter. With the aerosol introduction technique by LIBS, the detectable limit of 3 femtograms was obtained. Another sample introduction technique is *Electrospray Ionization*. Electrospray Ionization is a technique often used in mass spectrometry to generate ions where high voltage is applied to a liquid to create an aerosol (Huang J. et al., 2004). For electrospray ionization, volatile organic solvents are mixed with water, resulting in solvent evaporation (desolvation) for ion formation. Then this sprayed solutions can be analyzed by LIBS. *Pneuomatic and Ultrasonic Nebulization technique* is an other method for sample introduction. Analytes in liquid form for the nebulization process are vaporized with a nebulizer and allows the liquid substance to be delivered to the environment by steam. These converted analyte particles are trapped in aerosol droplets.
The pneumatic nebulization process is based on the Bernoulli principle, which allows creating a low pressure area with gas pressure in a cavity. This solution attracts the analyte and breaks it down in the gas stream through fine droplets. In an ultrasonic nebulizer, a piezoelectric crystal of high vibration frequency (usually 1-3 MHz) is used to create a liquid in a mobilizing chamber (Aras et al., 2012). Ultrasonic nebulization method was also studied by other groups to measure trace metal elements in liquids with LIBS (Zhong S., et al., 2015). Mn, Zn, Cu, Pb, Fe, Mg and Na are studied with that work. Also, in that work low energy laser pulses were used. *Hydride Generation Technique* is among the exemplary methods. Elements are converted into hydrate forms by forming method of hydride generation technique (Ünal S. and Yalçın Ş., 2010). When sodium boron hydride reagent (NaBH4 – strong reducing agent) combines with the elements to be analyzed in the acid solution, these elements turn into volatile hydrides. Some examples of these volatile hydrides of elements are As, Sb, Pb, Te, Se, Bi, Ge, Sn. Hydride formation reaction can be represented as;

$$3B\mathit{H}_4^- + 3H^+ + 4H_3AsO_3 \rightarrow 3H_3BO_3 + 4AsH_3\uparrow + 3H_2O$$

In this technique, energetic laser pulses are sent on to volatile hydrides, that are produced in a closed system, and plasma is formed. With this technique, sensitivity of many elements enhances by 10–100 folds.

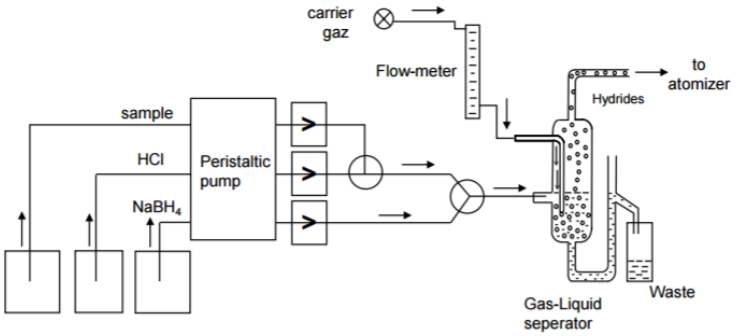

Figure 1.9. Setup for hydride generation technique

(Ünal S. and Yalçın Ş., 2010)

Simeonsson J. B. and Williamson L. J. have worked on hydride forms of some elements and characterized the laser induced plasma (Simeonsson J. B. and Williamson L. J., 2011). As, Sb and Se elements were reported with the limits of detection of 0.7, 0.2 and 0.6 mg/L, respectively.

Also, some methods are developed to convert the sample matrix from *liquid to solid phase* with the use of solid supporting materials like;

Filter paper- In 2008, Alamelu and team worked about a membrane-simultaneous determination of Sm, Eu and Gd in aqueous solution with the use of filter paper (Alamelu vd., 2008; Lee vd., 2012).

Graphite- Sub-ppm levels of boron in ground water samples by laser induced breakdown spectroscopy is determined using graphite as a substrate (Sarkar A. et al, 2010). Wood slices- Trace metal analysis in aqueous solution by LIBS is worked at 2008, by using a wood slice as a substrate to analyze trace metal samples (Chen Z. et al., 2008).

Ice – Liquid analyzing solutions can make freezing into an ice to anayze by LIBS were studied in 2001 (Cacares J. et al, 2001).

Polymer- Macronutrients in suspension fertilizers were mixed PVA and then dried to obtain the solid polymer film (Filho E. et al., 2017). The liquid to solid conversion

provide the LIBS analysis better. They worked with ICP-OES and also these results were predicted by LIBS with that technique.

Dry-droplet is another altenative technique to convert liquid to solid analysis. Such studies can be evaluated within the scope of Surface-Enhanced LIBS (SENLIBS) in the literature and these SENLIBS studies are also explained in detail in Chapter2.

1.3. Dry-Droplet Analysis by LIBS

An alternative technique for liquid analysis by LIBS and used by our group for different applications (Aras N. and Yalçın Ş., 2016). Dry-droplet analysis technique was likewise used by Bae and group for surface enhancement in liquid analysis with LIBS (Bae, 2015).

This method has three steps. First step is the loading step. For this step, some volumes of aqueous metal solutions are placed on the substrate. Second step is the drying step. approximately in 5 – 10 minutes, the sample dry at room temperature. This drying time changes with the volume of the sample and the concentration of the sample. The last step is the analysis. Energetic laser pulses are used to form plasma on dried residue to perform analysis step.

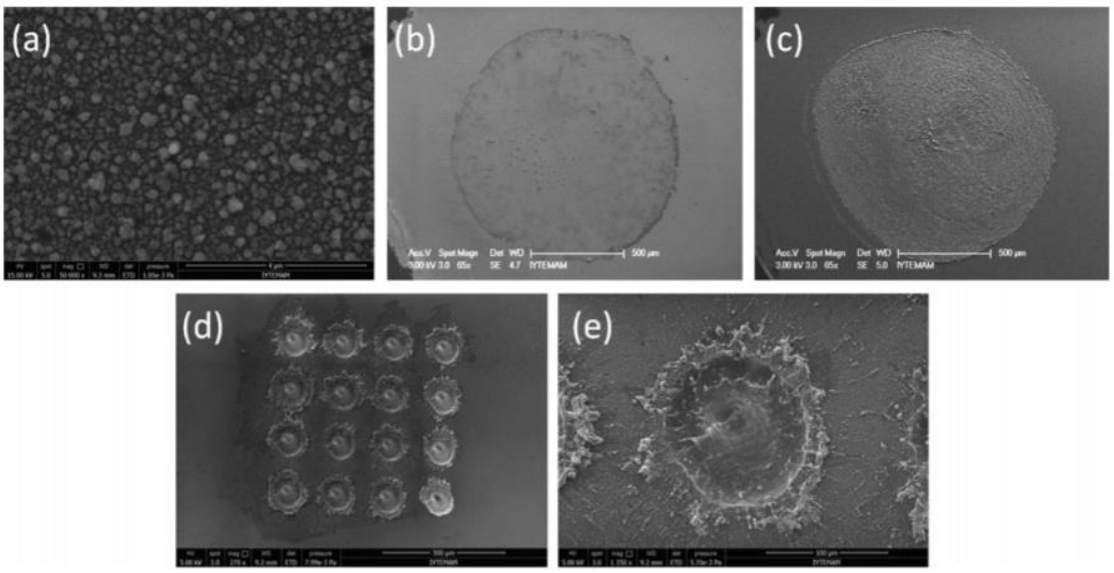

Figure 1.10. SEM images of a) Si+SiO2 surface, b) 500 nL dried droplet of 1 mg/ L copper solution, c) a crater after laser ablation of drying droplet by a 200 mJ single laser

pulse, d) 16 sequential sampling in a single droplet area with tightly focused laser pulses and, e) the enlarged view of one of the craters given in (d).

In this method, the liquid sample in a volume of 500 nL is loaded on the silicon surface and is let to dry. After drying, an image like Figure 1.10b is obtained and the resulting image after a single laser pulse is given in Figure 1.10c.

There are some certain examples of dry-droplet studies by LIBS in 2021. Matsumoto's team used porous silicone material as a target and carried out micro drop analysis with LIBS (Matsumoto A. et al, 2021). They worked on LIBS signal stability using this technique. In the same year, Sirven's group conducted dry droplet LIBS analysis (Sirven J.-B. et al, 2021). In this method, the matrix effect was worked in LIBS studies by preparing dry droplets.

1.4. Elements Studied: Lead, Copper, Chromium

Lead, Copper and Chromium are heavy metals extensively studied due to some environmental and health effects. Heavy metals are generally referred to as those metals which possess a specific density of more than 5 g/cm^3 and adversely affect the environment and living organisms (Järup, 2003).

Although these heavy metals are beneficial to the body to a certain extent and play a role in some mechanisms, they have certain limits and they must not be found in the body above these limits.

Heavy metals are a huge threat to the environment because they cause serious pollution and damage to the environment. (Nagajyoti P., *et al.*, 2010) . The most commonly found heavy metals in waste water include arsenic, cadmium, chromium, copper, lead, nickel, and zinc, all of which cause risks for human health and the environment (Lambert *et al.*, 2000). Certain organizations have determined these criteria so that heavy metals are not found in the body or in drinking water above the harmful limit.

Lead is a one of the important heavy metal, this metal causes some problems for environment and hazardous effect for human body. The sources of lead include mainly

waste water, drinking water, industrial processes, food and smoking sources. For example, thousands of tons of lead are released due to vehicle exhausts. From an environmental point of view, lead is a metal that does not have a positive effect on plants like other metals, even causes damage (Mathew B. B. et al., 2014).

Figure 1.11. Lead

Copper is an element that functions and should be in body functions. It is found in the drinking water, food and air, in this way it is supplied to the body. However, the presence of excess copper in the body causes danger. Copper poisoning can be caused by drinking or waste water, meals cooked in copper containers, or other environmental factors.

In cases where copper is excessive in the body, symptoms begin with complaints such as nausea, headache, diarrhea and vomiting and cause damage to the kidneys and livers. Copper poisoning also causes physical irritation to the eyes and nose.

Figure 1.12. Copper

Chromium is among the most abundant elements in the world. Chromium occurs in several oxidation states in the environment ranging from Cr^{2+} to Cr^{6+}. The most commonly occurring forms of Cr are trivalent- Cr^{+3} and hexavalent- Cr^{+6}, with both states being toxic to animals, humans and plants (Mohanty M. and Kumar P., 2013). Chromium is extensively used in industries such as metallurgy, production of paints and pigments, tanning, wood preservation, chemical production and paper production.

According to literature surveys, Cr(VI) has been found to be much more dangerous than Cr(III), since Cr(VI) enters the cells more readily than does Cr(III) and is eventually reduced to Cr(III). Because of its mutagenic properties, Cr(VI) is categorized as a group 1 human carcinogen by the International Agency for the Research on Cancer (Dayan A. and Paine J., 2001).

Figure 1.13. Chromium

Failure to control the exposure will result in severe complications in the future because of the adverse effects imposed by heavy metals.

Due to the fact that, all elements of the periodic table can be analyzed with Laser Induced Breakdown Spectroscopy, heavy metals present in a substance or in aquatic systems can also be analyzed both qualitatively and quantitatively. Although trace amount or very low concentrations of heavy metals may seem non dangerous for the human body to some extent, however, considering the accumulation of heavy metals in the organs of the human body even low levels of concentrations would be considered harmful.

The regulatory limit for lead in drinking water is set by US Environmental Protection Agency(EPA) as 15 ppb. The World Health Organization(WHO) says the lead and chromium content in drinking water should be 0.01 ppm, 0.05 ppm respectively.

Chinese Ministry of Health and The National Standards report the lead limit as 0.01 ppm, chromium limit as 0.05 ppm. World Bank has determined the lead limit in waste water as 0.1 ppm and the chromium limit as 0.5 ppm.

Unfortunately, the analytical figures of merits, e.g. LOD, sensitivity and linear range for LIBS are not high enough compared to other atomic spectroscopic techniques and one may not be able to determine heavy metals at trace amount concentrations. Thus, enhancement of the signal and hence detection limits of heavy metals requires some dedicated approaches to be applied and is crucial.

1.5 Aim of the Study

The purpose of this thesis study is to investigate silicon nitride coating thickness on silicon wafer substrates for enhanced sensitivity in dried nano-droplet analysis by LIBS.

As evidenced by the previous studies of our group, silicon nitride coated silicon wafer provides better enhancement of detection limits for some heavy metals compared to crystalline or silicon-oxide coated wafer (Aras N. and Yalçın Ş., 2018). Due to low reflectivity of the nitride coatings on Si-wafer surfaces, incoming laser beam absorbed more and rapid dissipation of the heat into the matrix resulted with an enhanced signal intensity of the heavy metals studied. An important detail for this previous study was that all silicon nitride coatings were about 300 nm thickness. This brought up a question, can silicon nitride coatings of different thicknesses improve the detection limits even further?

In order to answer this question, silicon substrates with different nitride thicknesses (75 nm, 300 nm, 450 nm and 1000 nm) were studied in terms of the LIBS signal enhancement, in this thesis study. Heavy metal solutions were loaded onto silicon nitride coated wafers of different thicknesses, and then sample on this wafers were analyzed by LIBS. In this perspective, lead, copper and chromium were studied as heavy metals.

After successful completion of the studies, a method would have been developed for the determination of heavy metals in polluted waters with better analytical figures.

CHAPTER 2

SURFACE ENHANCED LIBS (SENLIBS)

2.1. Theory of the SENLIBS

Surface Enhanced Laser Induced Breakdown Spectroscopy SENLIBS, is a technique that improves the analytical performance of the LIBS technique based on the use of different types of substrate surfaces for loading sample.

SENLIBS is based on the principle of interaction between the sample material and various target surfaces. SENLIBS is a method used to improve the accuracy, precision and linearity of the calibration curve in analyzes performed with LIBS. Due to these improvements, the limit of detections of the LIBS technique gets better.

The dry-droplet analysis method is very advantageous compared to other liquid analysis sampling techniques. With this technique, there is no need for steps such as intermediate solution phase change or sample preparation. In this way, analysis can be done directly by dropping the real sample without wasting time and wasting the product preparation.

This dried droplet methodology based on the use of several kinds of substrates like metallic or non metallic has been recently named as Surface Enhanced LIBS, SENLIBS, and several studies on this subject have appeared in the literature recently.

Aluminum substrate is used as a solid support for elemental analysis by LIBS (Aguirre et al., 2013). The enhancement observed on metallic substrates are explained on those surface as a hot and dense plasma. This energy translation is produced which engulfs the droplet and ‘enhances’ the LIBS signal. Also, oxide coated silicon wafer in which a higher surface area is available for immobilization of metal ions. Another SENLIBS study for trace metal determination was pioneered by Hidalgo. The samples to be analyzed in this study were dissolved with certain chemicals and dried on solid

substrate and analyzed with LIBS (Hidalgo M. et al., 2015). In a study conducted within the scope of SENLIBS in 2020, it is on the way to improve the signal intensity by making sampe preparation in a fixed area (Yang X. et al., 2020).

There have been studies in which metal substrates are used to increase the signal strength, but no studies have been conducted in this area with non-metallic substrates. In the previous study conducted by our group, oxide coated silicon wafer is used as a solid support (Aras and Yalcın, 2016). Studies performed on dried-droplet analysis. Silicon oxide coated silicon substrate has also some advantages compared to other wood or graphite type substrates due to the absence of impurities of some metal elements. The use of metallic (Aguirre et al., 2013) and non-metallic substrates (Aras and Yalcın, 2016) can be compared in terms of the dry droplet analysis by LIBS. For these two paper, manganese is the common for both, so manganese signal can be compared for this two work. Absolute detection limit was found as 49 ng/mL by using metallic substrate (aluminum substrate), but absolute detection limit was found as 6.7 ng/mL by using nonmetallic substrate (silicon wafer).

In recent years, a very popular approach has been taken to increase the signal intensity in liquid analysis with the use of metal nanoparticles (DeGiacomo A. et al., 2013).

Dried-droplet LIBS technique is an alternative liquid analysis technique in which the liquid sample, varying from microliter to milliliter, is dropped onto the appropriate substrate, dried, and the sample is transformed from liquid to solid and subsequently high-energy laser pulses are used for plasma formation (Cahoon E. and Almirall J., 2012). This technique, which does not involve complex sample preparation steps, is extremely simple and fast, the degree of laser-analyte, laser-substrate and analyte-substrate interactions occurring on the substrate surface with high-energy laser pulses sent on the sample is very effective on the signal intensity. Surface improvement studies have generally been carried out with the aim of monitoring the signal increase by using metal substrates (Zn, Al, MgO) (Lazic V. and Ciaffi M., 2017), and studies on the use of non-metal surfaces are almost nonexistent. The signal increase observed on metal surfaces is explained as the effective transfer of laser energy from the metal surface to the analyte. However, the uncontrolled distribution of the liquid droplet on the surface where it is dropped and the formation of non-homogeneous, irregular drops after drying, and sometimes the inability

to ensure the visibility of the drop on the surface are an important problem encountered on metal surfaces. In order to solve this problem, it has been shown that the structures formed by laser processing of the substrate surface keep the sample solution in place, prevent it from dispersing and provide homogeneity (Niu et al., 2016). In the literature, the only example of using a non-metal target in dry-droplet LIBS analysis is the laser structured grooves on the silicon wafer surface by Bae and his group to ensure the homogeneity of the dried droplet (Bae et al., 2015).

Metal analysis studies by LIBS, in our group have been previously carried out on silicon wafers using silicon-based coatings of certain thicknesses with different contents in order to find a suitable substrate in liquid analysis and to improve the determination limits with LIBS. In this context, the analytical performance of 300 nm silicon dioxide coated silicon wafer layer (SiO_2 + Si) and 300 nm silicon nitride coated silicon wafer layer (Si_3N_4 + Si) was performed by comparing it with pure silicon wafer (c-Si) (Aras and Yalçın, 2016; Aras and Yalçın, 2018).

Conditions such as the amount of the piece that the high-energy laser beam breaks off from the surface of the material, the mechanical and thermal effects applied to the layers, and the crater morphology on the material surface are directly related to many thermal, physical and chemical properties of the surface (Brown M. S. and Arnold C. B., 2010). It has been observed that coatings of different composition affect different physical events (thermal / photonics) during laser-material interaction. The results obtained in our previous studies show that the silicon nitride coated layer provides higher improvement on the signal intensity of Cd, Cr, Cu, Mn, and Pb elements compared to other substrates. The signal intensity increase observed on the surface covered with silicon nitride can be attributed to the heat transfer mechanisms of the silicon nitride material, besides its high absorption capacity, thanks to its superior thermal properties. Silicon nitride, as a kind of ceramic, is widely used in high temperature applications due to its superior thermal and mechanical properties such as high heat resistance, shock resistance, wear resistance, oxidation resistance and hardness (Ryklis E. A. et al., 1969). In addition, it is used as an anti-reflective and passivating layer on silicon solar cells with a wide band gap value of 5.0 eV (Zhu S. et al., 2013).

2.2. Silicon Nitride (Si_3N_4) Coating

Silicon nitride was obtained firstly in 1857 by Henri Etienne Sainte-Claire Deville and Friedrich Wöhler (Silicon Nitride. Wikipedia, The Free Encyclopedia). Silicone heated in a container placed in another container with carbon to reduce oxygen permeability. A product they called silicon nitride was reported, but without specifying its chemical composition. Chemical composition of the silicon nitride , Si_3N_4 , was reported by Paul Schuetzenberger in 1879. And over time, many scientists have obtained silicon nitride using different forms. Generally, silicon nitride can be obtained by heating silicon powder between 1300 – 1400 °C in nitrogen environment.

$$3\ Si + 2\ N_2 \rightarrow Si_3N_4$$

Also, silicon nitride can be obtained with many different techniques, like diimide route, carbothermal reduction etc. Another area that is most frequently used is to form a nitride layer for different purposes. For this subject, two main techniques are used, low pressure chemical vapour deposition (CVD) and plasma-enhanced chemical vapour deposition (PECVD) (Wafers, MicroChemicals)

2.2.1. Silicon Nitride; Production, Properties and Applications

Silicon nitride has been extensively studied in high temperature applications due to its superior thermo-mechanical properties like high temperature strength, good thermal shock resistance, fracture toughness and good oxidation resistance.

Due to all these strong characteristic properties, it is preferred in different fields for different applications. Another important property is wide band gap. Due to their wide band gap, (5.0 eV), silicon nitride thin-films on semiconductors are commonly employed for anti-reflection and passivation coatings for crystalline silicon solar cells.

Silicon nitride can be coated on a substrate by forming layers of different thicknesses for different purposes. This coating thickness can be determined as desired by changing some parameters of both chemical vapour deposition (CVD)and plasma enhanced chemical vapour deposition (PECVD) method.

Silicon nitride (Si_3N_4) has a very large usage area with all these characteristic features. This fields of application; in the construction of tools that need high mechanical and thermal stability, masking or etch stop material in wet and plasma etching processes due to its high chemical stability, masking material in silicon oxidation processes, anti-reflective coating in photovoltaics due to its adjustable refractive index, application of passivation or insulating layers in integrated circuits because of the chemical, electrical and optical properties (Wafers, MicroChemicals).

2.3. Light-Matter Interaction

Oscillating electromagnetic field of the the light and the matter can interact under four main topics; absorption, emission, transmission and reflection. If the matter is transparent, the energy will pass through it unchanged. If matter is a perfect reflector, the energy will not be changed except to change the direction in which it is moving. If electromagnetic radiation is absorbed by matter, then there is a transfer of energy from the radiant energy to the medium through absorption.

2.3.1. Reflection

Reflection is the process by which electromagnetic radiation is returned either at the boundary between two media (surface reflection) or at the interior of a medium (volume reflection).

The process through which light rays falling on the surface on an object are sent back is called reflection of light. Most surfaces do not totally reflect the light; they also absorb it.

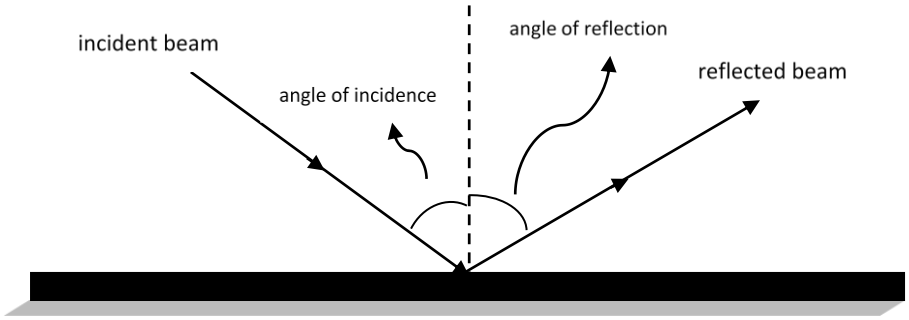

Figure 2.14. Reflection of the beam

This reflection can be of specular or diffuse reflection type.

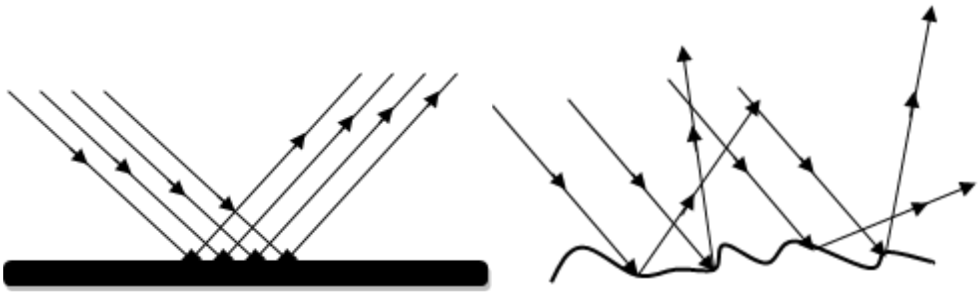

Figure 2.15. Diffuse reflection (left), specular reflection (right)

When the beam encounters a boundary like surface, and if this boundary can not absorb this beam, it reflects the waves away. In that way, reflection of light is observed.

Briefly, this can be said that the photons of light and the electrons on the surface of the material is caused reflection. Some materials completely reflect the light or completey absorb light, but also there have been other materials that reflect the part light light while transmitting the rest.

2.3.2. Refraction

Refraction is the change in direction of a wave passing from one medium to another medium.

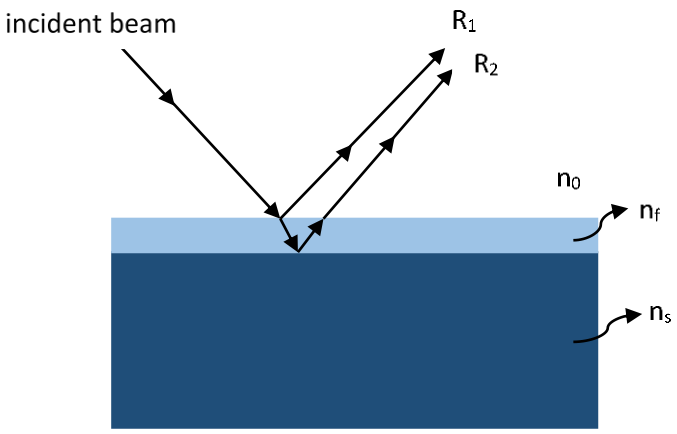

Figure 2.16. Refraction of the beam

The index of refraction of a thin film (n_f) needed for complete cancelation of the reflected beams can be found by using the refractive indices of the incident medium (n_0) and the substrate (n_s).

$$n_f = \sqrt{(n_0 n_s)}$$

Since LIBS experiments are mostly performed in air so the inciden medium refraction index, n_0 is equal to approximately 1. When we look at the materials that we use, refraction index of silicone wafer is used as a substrate n_s. This n_s value is equal to 4.15. The silicon nitride refractive index, which we choose for coating, is 2.05. As a result of this formula, the result of the n_f value should be 2.05.

$$nf = \sqrt{(n0 * ns)}$$

$n_f = (1*4.15)^{1/2} = 2.04$

According to the refraction values, it is concluded that the silicon nitride is correct coating material in formulation as an anti reflection coating.

2.3.3. Anti-Reflection Coating (ARC)

It is undesirable to have a reflection of the light coming on some substances, and specific materials can help in order to reduce these undesired reflections.

Anti-Reflection Coating (ARC) has a wide range of applications in the area of light optical systems. For instance, ARC is used on corrective lenses, camera lenses and on solar cells to get rid of unwanted reflection and low loss of light. In the telescopes and microscopes, the reflection of the light should be the least amount in order to make the image clear. Again for the same purpose, coatings are also used on the eyeglasses. With all these usages, the efficiency of optical systems is improved by low reflections.

Thin film anti-reflection coatings greatly reduce the light loss by making use of phase change and the dependence of the reflectivity on index of refraction. ARC can be made by single layer, double layer or multi layer coatings. TiO_2, SiO_2, Si_3N_4, MgF_2, ZnS, Al_2O_3 etc. are used as a ARC coating. In terms of solar cells, silicon nitride or titanium dioxide coatings in nano scales are used to reduce reflectance.

There are two causes of optical effects due to coatings, often called *thick-film* and *thin-film* effects.

Antireflective effects from thin film coatings arise when the coating is between a quarter and a half of a wavelength of light. This effect reduces the reflection on the surface because of its destructive interference. For thin films, the angle at which the light strikes the surface is often important in determining how much light is absorbed.

On the other hand, antireflective effects using a thick film occur because of the difference in the index of refraction between the coating and the layers either side of it. Thick film coatings are not dependent on the specific thickness, but the coating needs to be thicker than a wavelength of light to work (Critchley L., 2018). The anti-reflection coating used in this thesis is silicon nitride with coating thicknesses of 75 nm, 300 nm, 450 nm and 1000 nm. Considering the laser wavelength used is 532 nm, it can be expected to have not only thin film effect, but a thick film effect is observed, as well.

CHAPTER 3

EXPERIMENTAL STUDY

3.1. LIBS Experimental Set-Up

The experimental LIBS sytem used throughout this thesis study is composed of three main parts as; laser source, optical materials and detection systems. Laser source is the Neodymium-doped Yttrium Aluminum Garnet (Nd:YAG) type of laser with 10 ns duration time and 10 Hz. Repetition rate. The laser beam out of the laser source (Quanta-Ray Lab-170, Spectra- Physics, California- USA). is reflected by mirrors and focused on to the target material by some lenses (1'' OD, coated, 532 nm reflective, plano-convex lens, New Focus, Darmstad-Germany). The plasma emission formed on the target material is collimated and focussed by a pair of lenses (2 " OD, 532 nm reflective, plano-convex lens, New Focus) on to the tip of a fiber optic cable (Ocean Optics, P600-2UV-VIS,600 μm diameter) and transmitted to the entrance slit of the spectrograph (an Echelle spectrometer equipped with a charged coupled device (ICCD) (iStar DH734, Andor Inc.)). Plasma emission is analyzed by AndorSolis software.

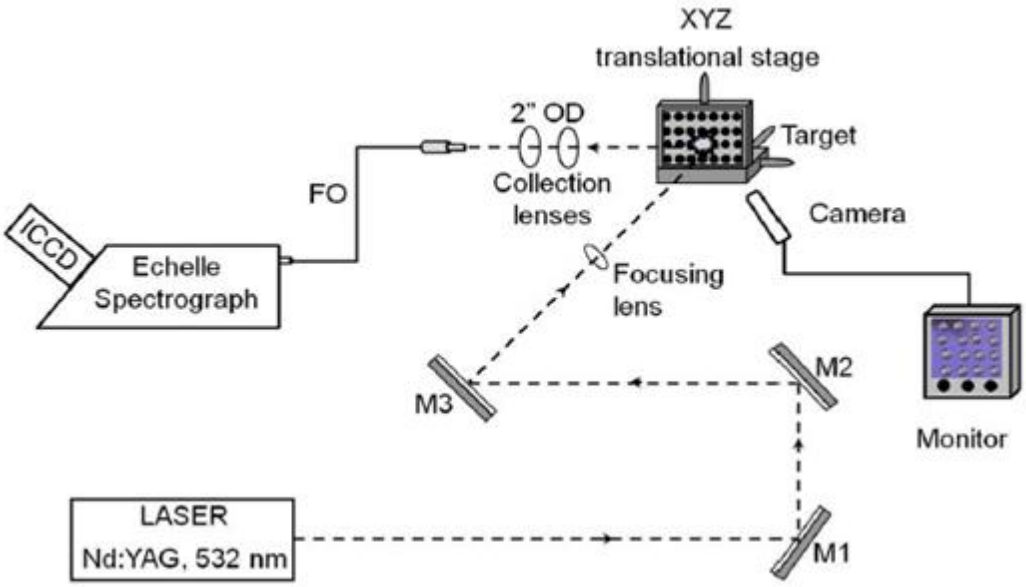

Figure 3.17. Block Diagram of the Experimental LIBS Set-up

(Aras and Yalçın, 2018)

3.2. Substrates and Chemicals

3.2.1. Silicon Nitride Coated Wafers and Apparatus

Boron doped Si-wafers, as is shown in Figure 3.18(a-d), of 4 " OD, 525 +/- 25 micrometer thickness, and coated with 75 nm, 300 nm, 450 nm and 1000 nm silicon nitrides by low pressure chemical vapour deposition method were obtained from *MicroChemicals GmbH*.

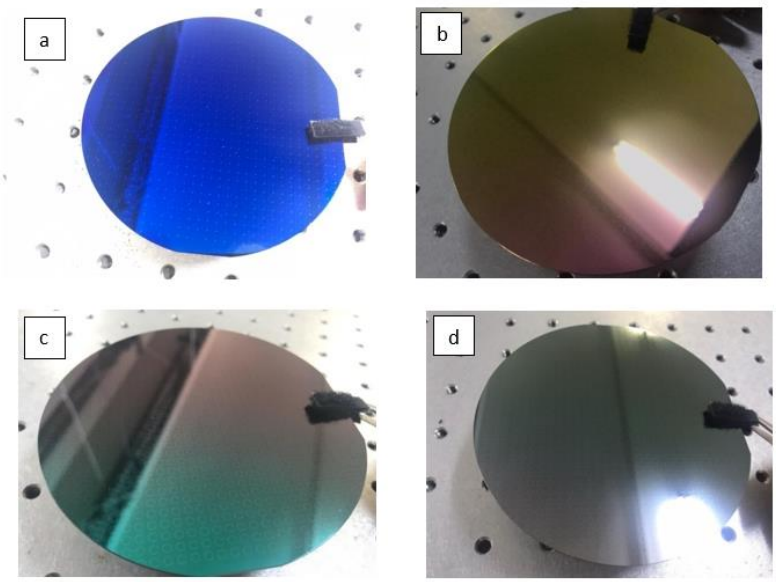

Figure 3.18. a) 75 nm b)300 nm c) 450 nm d) 1000 nm Si_3N_4 coated silicon wafers

Wafers were laser marked with 2mm diameter circles to identify the loading area of 500-nanoliter samle droplets. This process was done in *İzmir Laseral* company. The laser used to make these 2mm frames is a type of fiber laser.

Since silicon wafers with different coating thicknesses is used during the analyzes, a sample holder apparatus has been developed to ensure that the sample to lens distance stays unchanged (Figure 3.19).

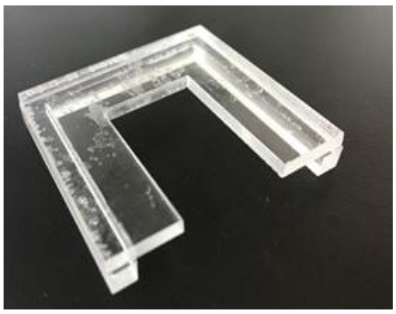

Figure 3.19. Apparatus to fix wafers of different thicknesses at the same sample to lens distance

3.5. Chemicals and Standart Solutions

Standard solutions of single heavy metal elements (Pb, Cr, Cu) were used to study the experimental optimization parameters and for the construction of calibration graphs, by suitable dilution.

Figure 3.20. Heavy metal solutions

Detection limits for each element were calculated from the statistical analysis of the calibration graphs drawn. In order to evaluate the analytical performance of the technique for dry droplet analysis, various heavy metal solutions, Figure 3.20, 3,21 and 3.22, as reference water samples and contaminated water samples were utilized.

Figure 3.21. Multielement solutions

AccuStandard – Technology Reference Materials (TRM), Trace Metal Standard 1, Plasma Emission Standard (ICP) and European Reference Materials (ERM) - CA011c Hard Drinking Water UK– Sample:0653 – Certified Reference Material –LGC6026 solutions and High Purity Solution DWPS-A-100 solutions were also used as the multielements solutions. With these multielement water samples, matrix effect on Cr, Cu and Pb elements has been studied.

Figure 3.22. SLRS4 Riverine water solution

Real water sample, SLRS4 riverine water, shown in Figure 3.22, with very low concentrations of the heavy metals, and market drinking water, OZSU, were used within

the scope of the spiking studies. The validation studies of the method with these solutions were presented and parameters such as recovery and percentage errors were determined.

3.3. Dry Droplet Analysis

In this study, liquid samples of definite volumes (500 nL) were loaded directly on the silicon nitride coated wafers, Figure 3.23, with no sample preparation method applied. The dry-droplet methodology consisted of 3 steps. First Step is the loading step. The 1st picture of Figure 3.23 shows that 500 nanoliters sample solution or standard solution is loaded onto the silicon nitride coated wafer. Second Step is the drying step. 2nd picture shows the residues of 500 nanoliters liquid samples that are dried at room temperature in about 5 minutes. Last step is the analysis step. 3rd picture shows the craters formed on the Si-wafer substrates after laser pulses are sent on to them fır LIBS analyses.

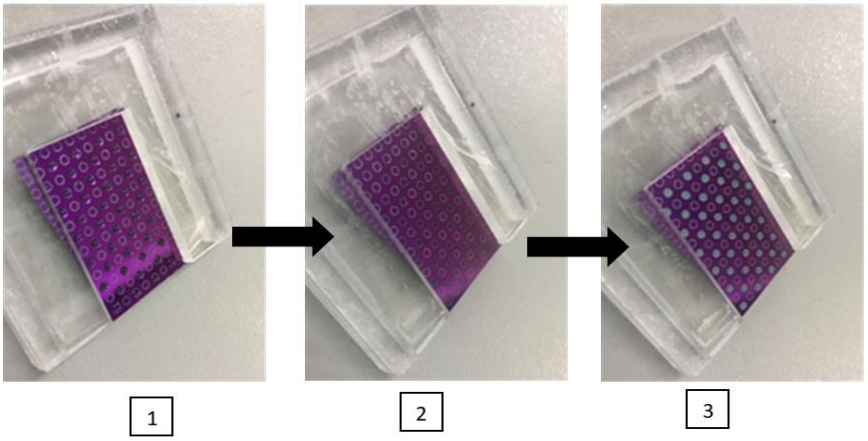

Figure 3.23. Dry Droplet Analysis

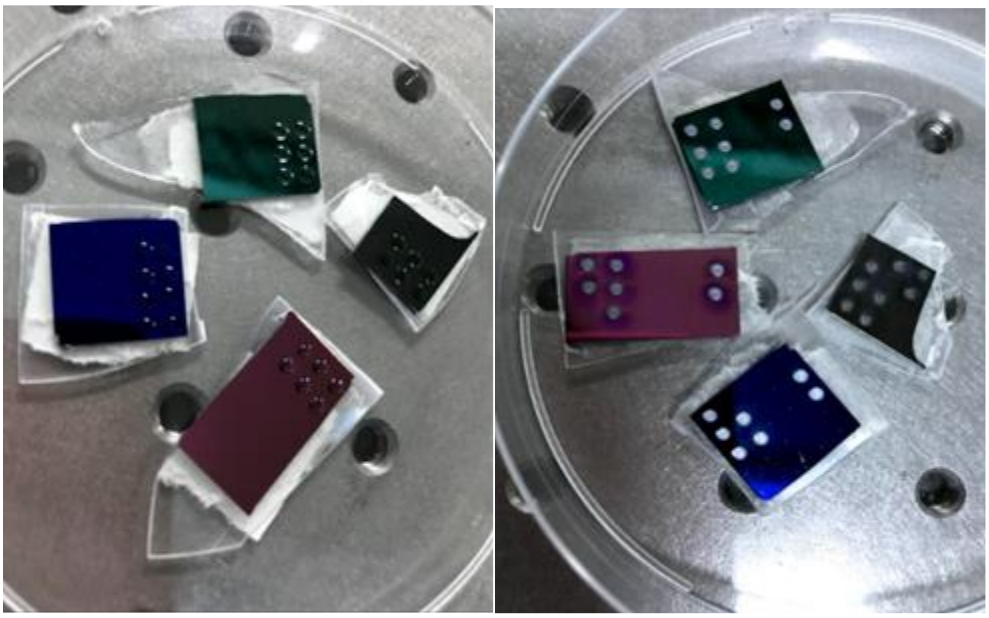

Figure 3.24. 75 nm (blue), 300 nm (pink), 450 nm (green) , 1000 nm (grey) silicon nitride coated wafers , while the drops are loaded (left), after dry-droplets are analysed by LIBS (right).

As the reflectivity of surfaces with different coating thickness changes, this can be easily distinguished from their colors, as is seen in Figure 3.24. The left photograph of Figure 3.24 shows freshly loaded droplets on the substrates, whereas, on the right, photographs of the samples analyzed by laser pulses for LIBS analysis are shown.

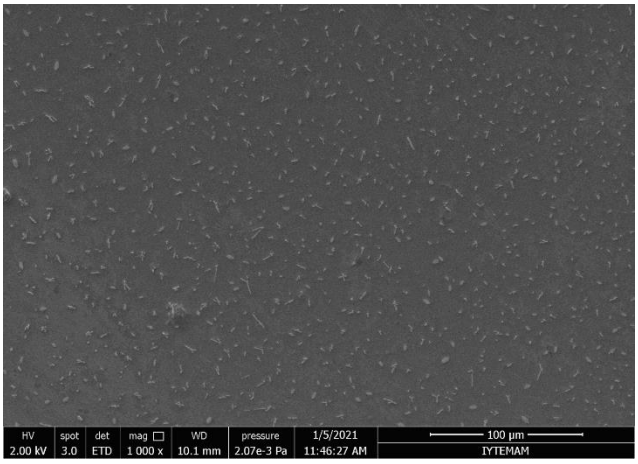

Figure 3.25. SEM image of 500 nL dried droplet of the heavy metal sample

Scanning Electron Microscope(SEM) images of the region after the standard heavy metal elements are dried on the wafer were also studied. Figure 3.25 shows the SEM image of a 500 nanoliter sample solution loaded and dried on the substrates. Almost

homogeneous distribution of crystals from the dried droplets of aqueos solutions was observed.

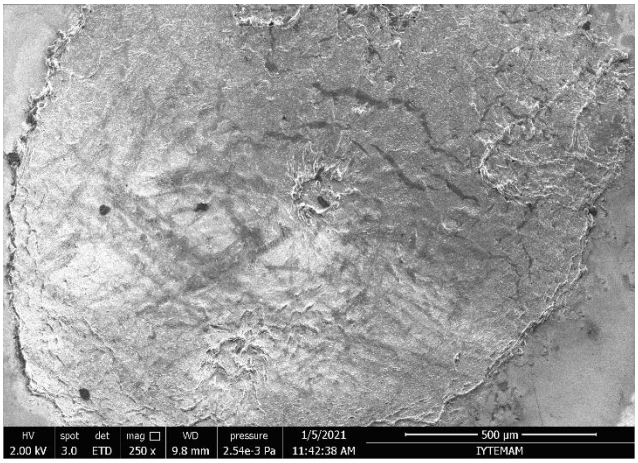

Figure 3.26. SEM image of the dried droplet sample after analyzed with LIBS

The SEM image seen in Figure 3.26 is from the analysis of a dry droplet is exposed to energetic laser pulses four times in a row for LIBS analysis.

3.4. Optimization Studies of LIBS Set-Up

The first step in optimizing the LIBS system is to adjust the output of the laser light from the laser source with the best efficiency. For this, it is necessary to adjust the positions of mirrors and lenses in order to reflect the light with mirrors in the most efficient way and to focus it with the lenses. The second step is to adjust the position of the focusing lens to a laser beam diameter of 2 mm by moving it closer or further from the sample. 2 mm represents the diameter of the droplet loaded. The next step is to adjust the position of the head of the fiber cable that will transmit the plasma emission to the detector for each element separately. As the last step, the LIBS system parameters delay time, gate width, energy of laser pulse, detector gain values must be optimized for each element.

The *delay time* is the parameter that describes how long after the detector open its eye when the laser beam hits the sample. *Gate width* is the variable that indicates how long

the detector opens its eye to collect data. The laser pulse *energy* study is the optimization of the laser beam energy in terms of signal strength of analyte specie. *Gain* value is the relative magnitude that represent the detector voltage applied.

CHAPTER 4

RESULT AND DISCUSSION

4.1. Reflectance Measurements

Silicon wafer has high surface reflectivity and a thin layer of material coated on it provide a means to decrease the reflectivity. Due to its antireflective feature, silicon nitride coatings are used to reduce surface reflection and light loss hence efficiency increases. The thickness of the antireflective coating material is important because of the interference effects (constructive and destructive) that occur in the coating material. Within the content of this thesis study, in order to investigate the effect of coating thickness on LIBS signal strength silicon nitride coatings of different thicknesses were utilized. Reflectance spectra, between 200 nm to 800 nm, for each substrate of different thicknesses were obtained, and given in Figure 4.27.

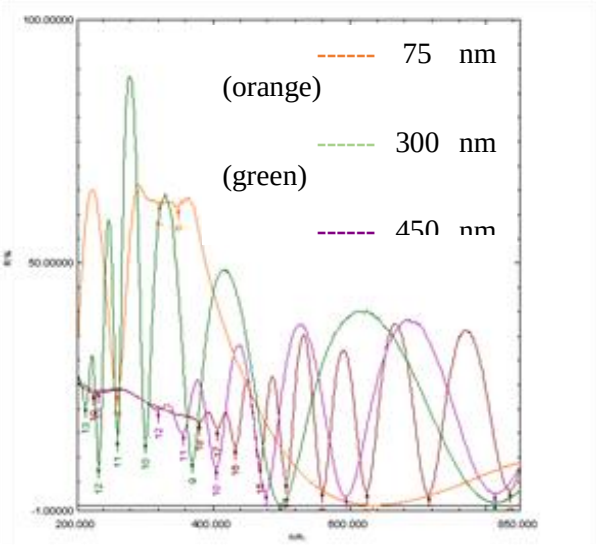

Figure 4.27. Si_3N_4 (75 nm, 300 nm, 450 nm, 1000 nm) reflectance measurement spectrum in any thickness from 200 nm to 800 nm

As can be seen from the spectra, wafers with different thicknesses exhibit different reflectivities. For a closer look, reflectivity data within the spectral range of interest around 532 nm, Nd:YAG laser wavelength, are tabulated in Table 4.1.

Table 4.1. Reflectivity data for the substrates with different coating thicknesses within the spectral range of interest around 532 nm

Wavelength nm.	75nm RawData	300 RawData	450nm RawData	1000nm RawData
536	5,75104	16,61377	36,10077	33,9447
535	5,89447	16,1377	36,45325	34,53064
534	6,01349	15,48157	36,53412	34,90295
533	6,1264	14,84528	36,54327	35,12573
532	6,27747	14,27002	36,7569	35,1944
531	6,44836	13,66119	37,10938	35,04028
530	6,58417	13,03864	37,22687	34,68323
529	6,71082	12,45575	37,30011	34,31549
528	6,8573	11,87744	37,40997	33,76312

At the wavelength of 532 nm, reflectivity increases with coating thickness and minimum reflectivity is obtained for the substrate with minimum coating thickness of 75 nm. In order to support this experimental results, the thickness of the antireflective coating for minimum reflection was calculated, theoretically, from the equation $d = \lambda_0 / 4n$

where d: optimum ARC thickness (um),
λ: wavelength of the radiation
n: refractive index of the material used.

For silicon nitride coating, refractive index value of 2.05 and 532 nm wavelength from a Nd: YAG laser is substituted in the formula, 65 nm coating thickness value is found as optimum thickness. This value is close to the one (75 nm) we have considered to evaluate within this thesis study. 75 nm coating is the thinnest silicon nitride coating commercially available, and is used throughout the experiments for a comparative study.

4.2. Optimization of the Instrumental Parameters for Heavy Metals

In the experiments carried out to determine the optimum conditions to be used in heavy metal analysis by LIBS, the variation of signal intensity with; delay time, Td, data acquisition interval (gate time), Tg, and laser pulse energy were studied for each element. For optimizing one parameter, the others kept constant. In delay time optimization, data acquisition time and laser pulse energy were kept constant.

4.2.1. Optimization of Chromium – Cr(I) signal

For chromium element optimization studies, heavy metal solution of 100 ppb concentration were used. 500 nanoliter aqueous chromium solution were loaded onto 300 nm silicon nitride coated wafers, and dried at room temperature within 5 minutes. These dried droplets were analyzed by LIBS for maximizing chromium emission signal at 428.9 nm wavelength.
To optimize the delay time, the gate width was kept constant at 20 microseconds. For gate width optimization, the delay time used as 0.5 μs. For laser pulse energy optimization, a range between 90 - 190 mJ has been studied.

Figure 4.28 shows the variation of LIBS signal for Cr at 428.9 nm emission line, with respect to change in delay time, gate width, and laser pulse energy.

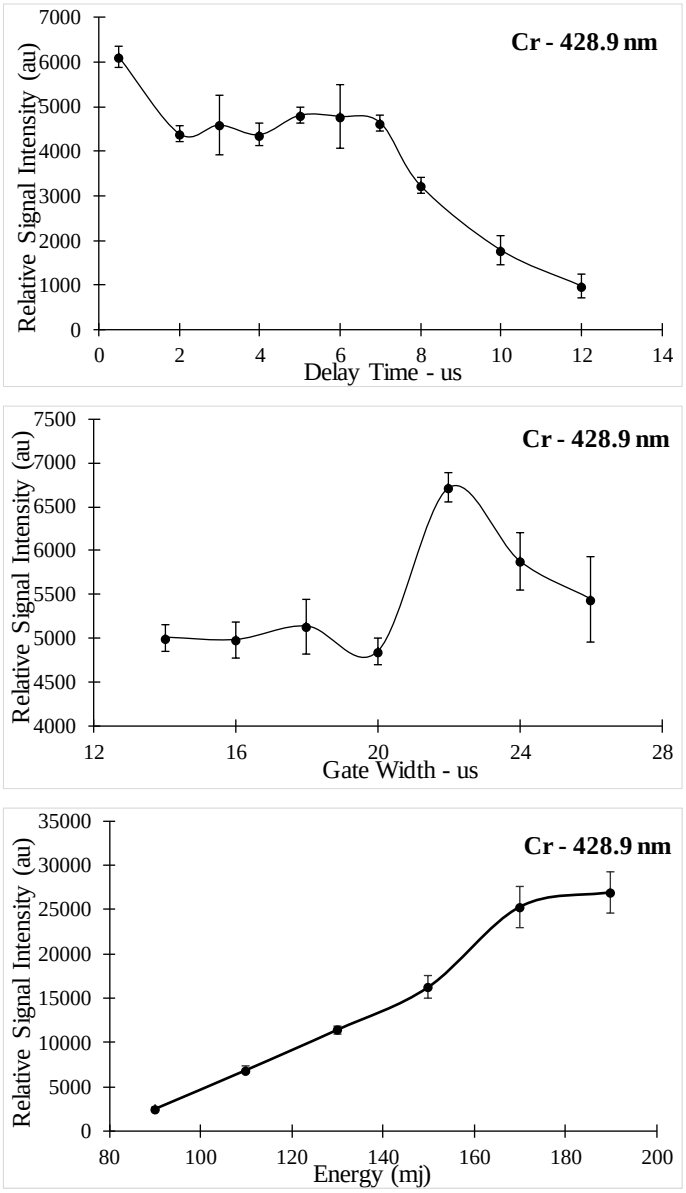

Figure 4.28. 500 nL 100 ppb Chromium solutions were dropped onto 300 nm Si_3N_4 coated wafers, and optimized about delay time, gate width and laser energy by LIBS

In this study, the signal with the emission of the chromium element at a wavelength of 428.9 nm was investigated. This emission diagram is shown in Figure 4.29.

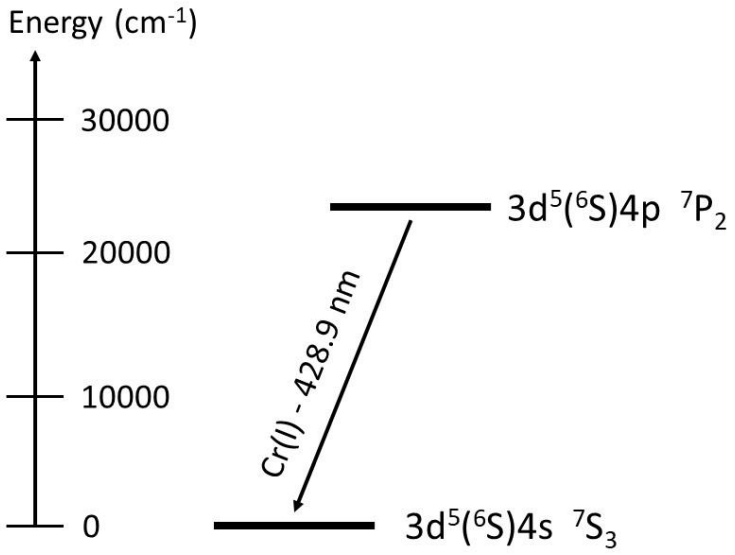

Figure 4.29. Grotrian diagram of Cr(I).

4.2.2. Optimization of Copper – Cu(I) signal

For copper element optimization studies, heavy metal solution of 100 ppb concentration were used. 500 nanoliter aqueous copper solution were loaded onto 300 nm silicon nitride coated wafers, and dried at room temperature within 5 minutes. These dried droplets were analyzed by LIBS for maximizing copper emission signal at 324.7 nm wavelength.

To optimize the delay time, the gate width was kept constant at 1 millisecond. For gate width optimization, the delay time used as 300 ns. For laser pulse energy optimization, a range between 90 - 210 mJ has been studied.

Figure 4.30 shows the variation of LIBS signal for Cu at 324.7 nm emission line, with respect to change in delay time, gate width, and laser pulse energy.

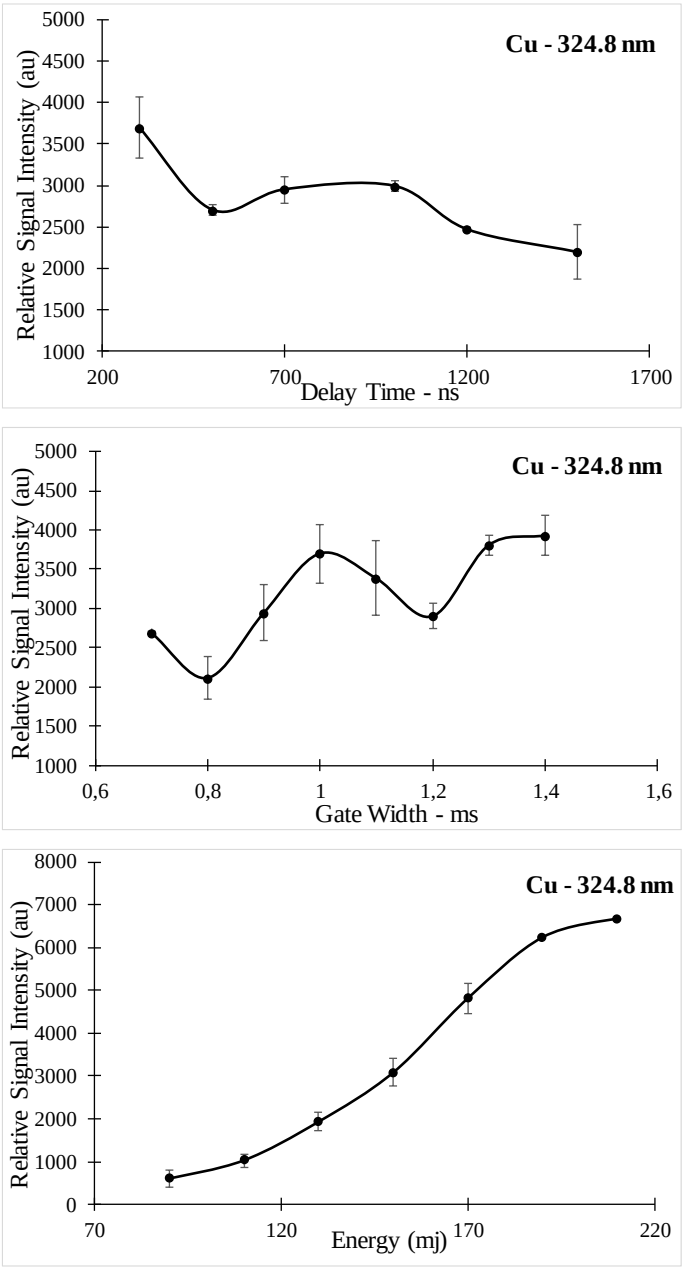

Figure 4.30. 500 nL 100 ppb Copper solutions were dropped onto 300 nm Si_3N_4 coated wafers, and optimized about delay time, gate width and laser energy by LIBS

In this study, the signal was investigated by the emission of copper element at a wavelength of 324.7 nm. The transitions and energy levels here are shown in Figure 4.31.

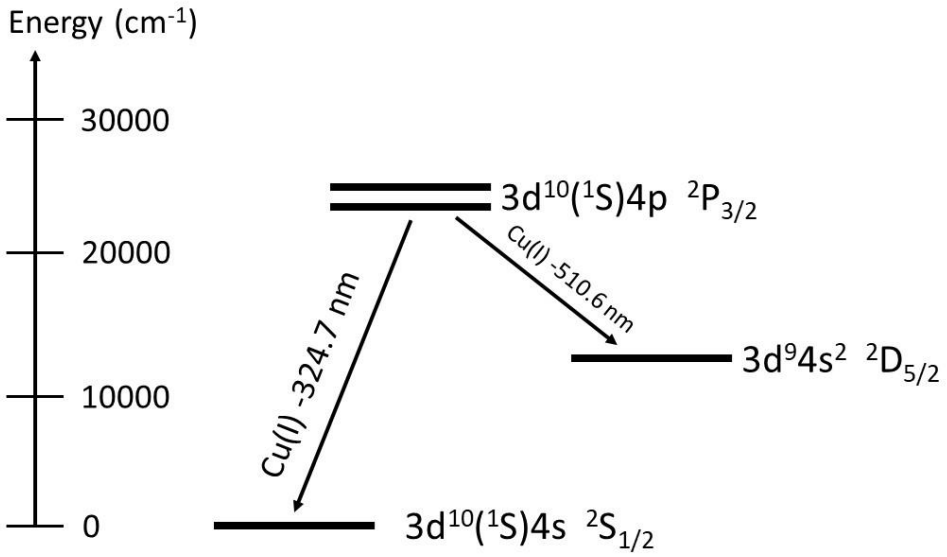

Figure 4.31. Grotrian diagram of Cu(I).

4.2.3. Optimization of Lead – Pb(I) signal

For lead element optimization studies, heavy metal solution of 100 ppb concentration were used. 500 nanoliter aqueous lead solution were loaded onto 300 nm silicon nitride coated wafers, and dried at room temperature within 5 minutes. These dried droplets were analyzed by LIBS for maximizing lead emission signal at 405.8 nm wavelength.

To optimize the delay time, the gate width was kept constant at 500 microseconds. For gate width optimization, the delay time used as 2 us. For laser pulse energy optimization, a range between 90 - 190 mJ has been studied.

Figure 4.32 shows the variation of LIBS signal for Pb at 405.8 nm emission line, with respect to change in delay time, gate width, and laser pulse energy.

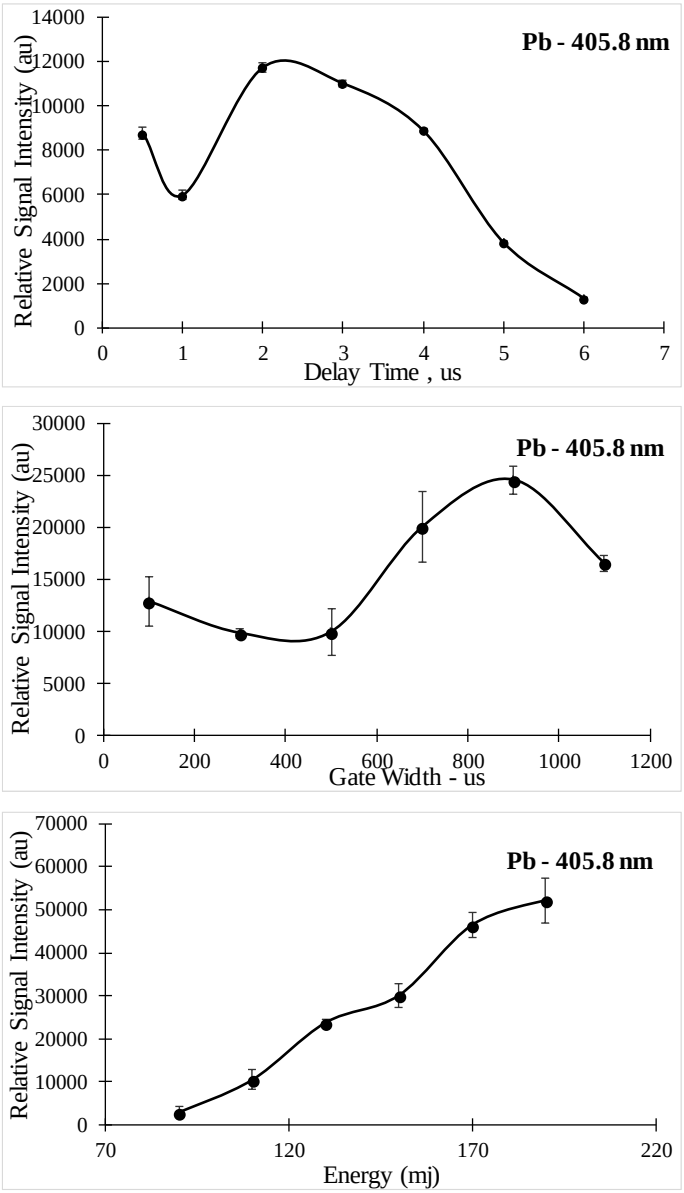

Figure 4.32. 500 nL 100 ppb Lead solutions were dropped onto 300 nm Si_3N_4 coated wafers, and optimized about delay time, gate width and laser energy by LIBS

In this study, LIBS was studied on the emission of lead element at a wavelength of 405.8 nm. The transitions and energy levels here are shown in Figure 4.33.

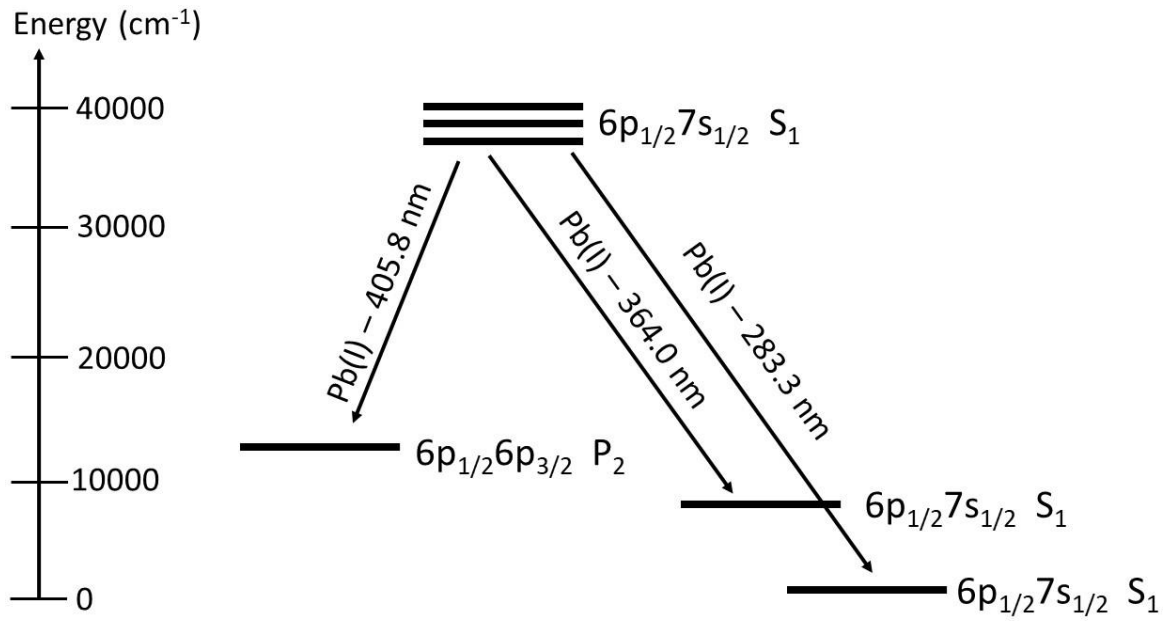

Figure 4.33. Grotrian diagram of Pb(I).

The optimum conditions obtained from the optimization studies, for the elements Cr, Cu and Pb, are listed in Table 4.2., below.

Table 4.2. Optimum parameters for Cu(I), Cr(I) and Pb(I)

	Delay Time , T_d	Gate Width , T_g	Energy , E (mj)	Wavelength, (nm)
Cu (I)	300 ns	1400 µs	130	324.8
Cr (I)	0.5 µs	22 µs	130	428.9
Pb (I)	2 µs	900 µs	130	405.8

4.3. Representative LIBS Spectra

After optimization studies are completed, typical LIBS spectra under optimum experimental conditions were obtained, Figure 4.34 for Cr, Figure 4.35 for Cu and Figure 4.36 for Pb. Analyte emission signals within relevant spectral region at the most descriptive wavelength, 424-430 nm for Cr, are also presented enlarged as; a) 300 nm, b) 75 nm, c) 450 nm and d) 1000 nm Si_3N_4 coated surfaces.

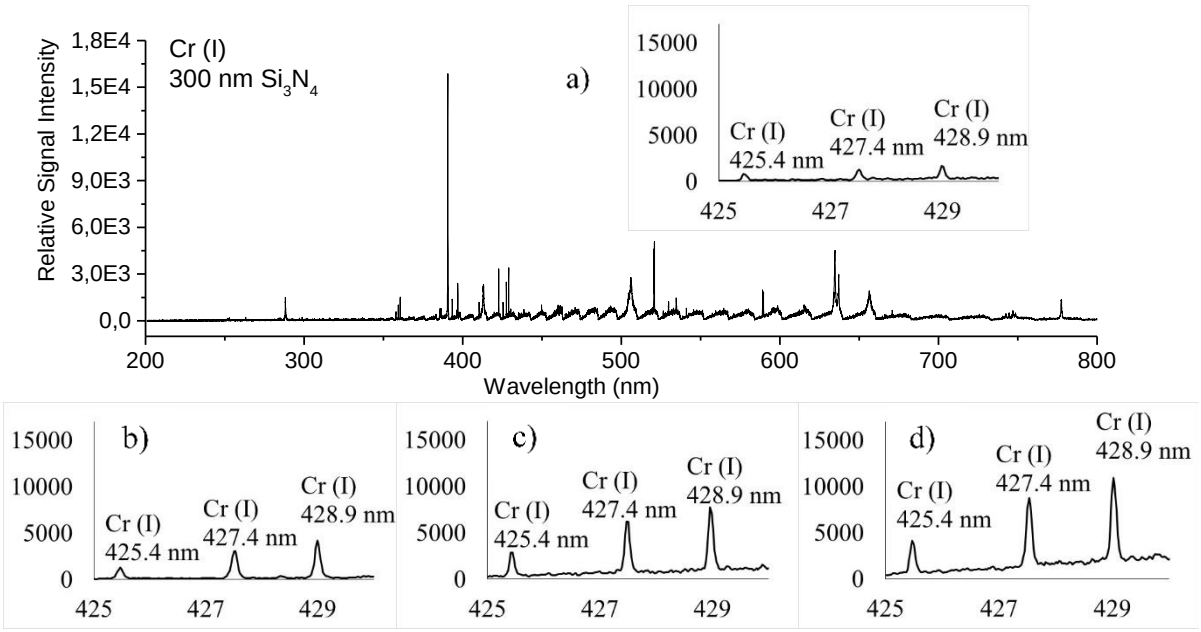

Figure 4.34. Descriptive LIBS spectra obtained from plasma generated by laser pulses of 130 mJ energy followed by drying of 500 nL Cr solution at a concentration of 50 microgram loaded onto a) 300 nm, b) 75 nm, c) 450 nm and d) 1000 nm Si_3N_4 coated surface

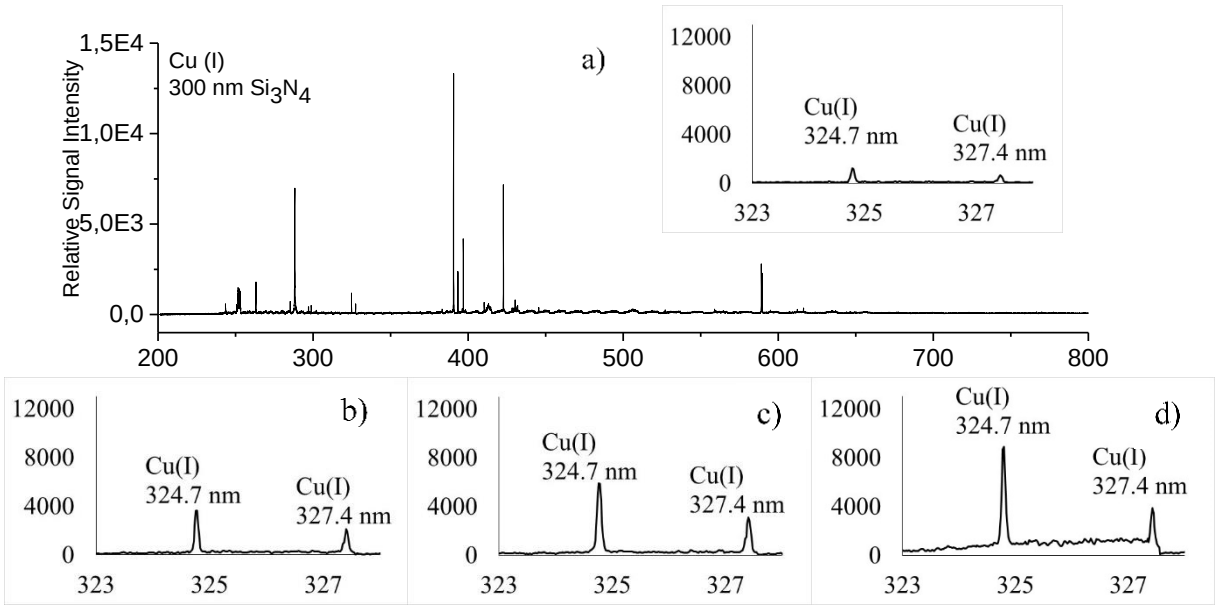

Figure 4.35. Descriptive LIBS spectra obtained from plasma generated by laser pulses of 130 mJ energy following drying of 500 nL Cu solution at a concentration of 50

microgram / L loaded onto a) 300 nm, b) 75 nm, c) 450 nm and d) 1000 nm Si_3N_4 coated surfaces

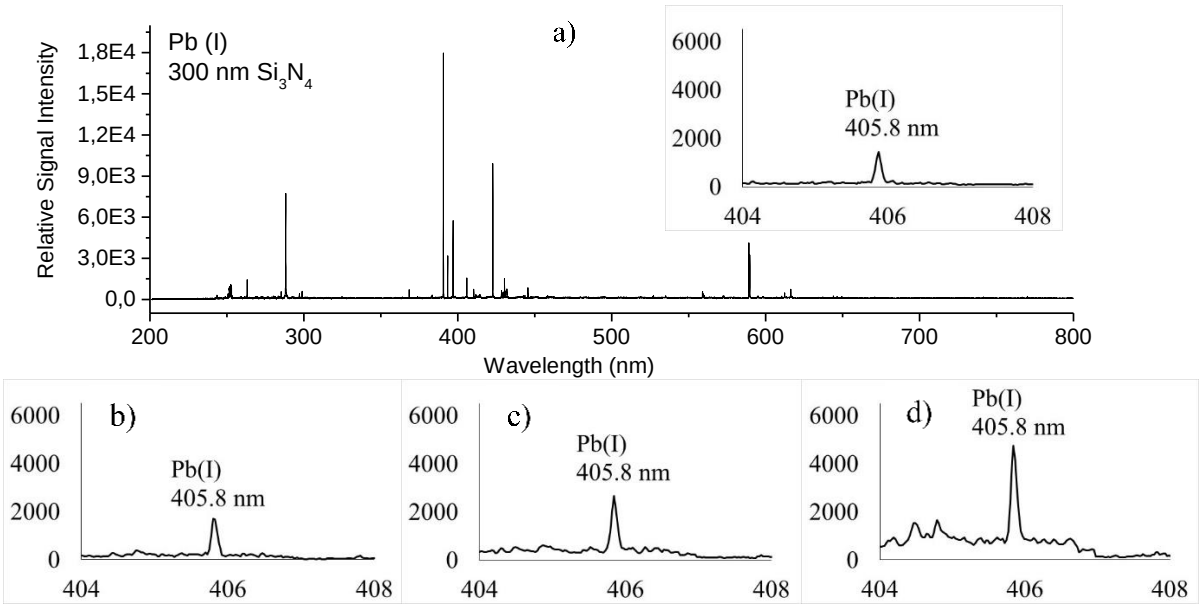

Figure 4.36. Descriptive LIBS spectra obtained from plasma generated by laser pulses of 130 mJ energy following drying of 500 nL Pb solution at a concentration of 50 microgram / L loaded onto a) 300 nm, b) 75 nm, c) 450 nm and d) 1000 nm Si_3N_4 coated surfaces

The observed LIBS signal intensities at 405.8 nm for lead, 324.7 nm and 327.4 nm for copper, 425.4 nm, 427.4 nm and 428.9 nm for chromium are given separately for each coating thickness in each spectrum.

Using optimum parameters for each element, 500 nL heavy metal solutions of the analyte element was loaded onto the wafers and analyzed by LIBS. In this analysis, the average of the signal from 3 separate droplets each is from the accumulation of 4 laser pulses were used.

4.4. Variation of signal intensity with Si_3N_4 coating thickness

In order to determine the effect of Si_3N_4 coating thickness on the signal intensity, the signal intensity of each element at the selected wavelength was determined for each

nitride coating thickness. For this purpose, droplets of lead, copper and chromium metal with 70 ppb concentration in the volume of 500 nanoliter were loaded on silicon nitride coatings of different thicknesses and then exposed to high energy laser pulses.

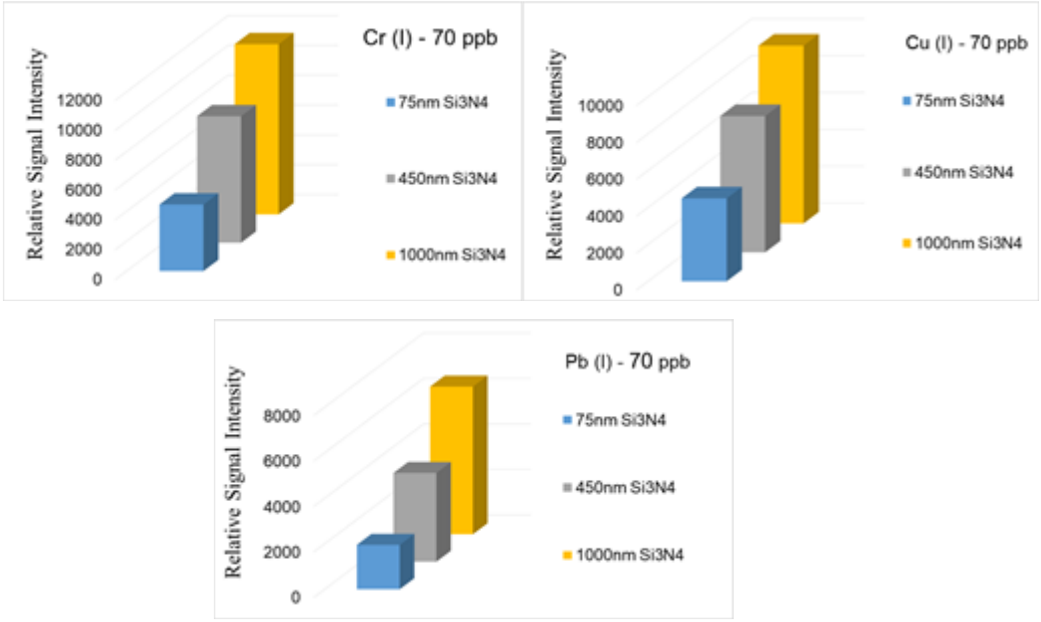

Figure 4.37. The variation of signal intensities at different silicon nitride coating thicknesses in dry drop analysis of Pb, Cu and Cr solutions.

As is observed in Figure 4.37, the relative signal strength is the highest with 1000 nm coated Si-wafer substrates, for all three elements. LIBS signal intensities of the studied metals observed in different thicknesses were also compared with the signal intensities obtained by using 300 nm Si_3N_4 coated wafers, used in our previous studies. The enhancement factor in signal intensities obtained in this way is given in Table 4.3. The relative increase factor obtained with 1000 nm silicon nitride coated layer is higher than other coatings, being around 4.5 times maximum.

Table 4.3. Ratio of signal intensities of heavy metal elements (100 ppb) with wafers of different thickness to signal intensity with 300 nm silicon nitride coated wafer

	75 nm Si_3N_4	450 nm Si_3N_4	1000 nm Si_3N_4
Pb (I)	1,26	2,39	4,52
Cr (I)	1,27	2,18	3,0
Cu (I)	2,29	3,35	4,48

After this optimization and general LIBS study, the plasma temperature values obtained during the study were calculated.

With the optimum conditions, an average plasma temperature of 16837 K was obtained with chromium work, an average of 13034 K with copper work and an average of 13682 K with lead work. Since the theoretical temperature of the LIBS plasma in the past is between 10 thousand and 20 thousand, it can be said that we are in the right conditions within the scope of this study.

Chromium studies are shown in Figure 4.38 as an example of calculated plasma temperature studies.

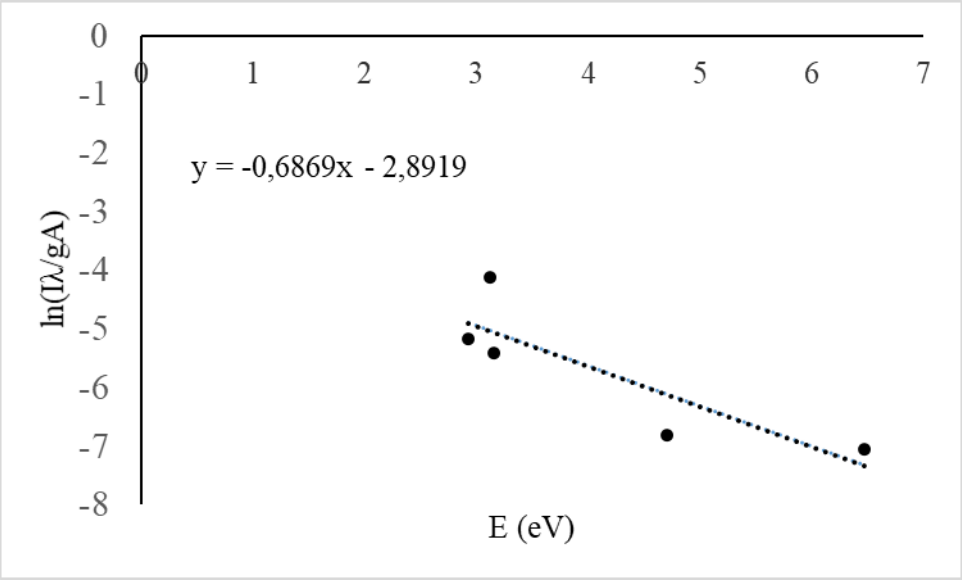

Figure 4.38. Plasma temperature study

The T value is reached by using the equation T=1/slope*k on the slope obtained by drawing the graph of energy (eV) versus ln(Iλ/gA). With the result of the calculation here, T is obtained as 16837 K.

Table 4.4 shows how the plasma temperature value changes in different silicon nitride coatings over the studies performed with copper. In addition, electron density values obtained due to these changing temperature values are also seen in the same table.

Table 4.4 Plasma temperature and electron density values for copper

	75 nm Si_3N_4	300 nm Si_3N_4	450 nm Si_3N_4	1000 nm Si_3N_4
Plasma Temperature	11075 K	11566 K	12071 K	13034 K
Electron Density	$9.4*10^{15}$	$9.6*10^{15}$	$9.8*10^{15}$	$1.02*10^{16}$

$Ne \geq 1.6*10^{12}*(\Delta E)^3*(\sqrt{T})$ equation was used to calculate the electron density values in Table 4.4. T means the plasma temperature, ΔE is the energy difference of the copper levels. When we look at the electron density value at 1000 nm, we can talk about local thermal equilibrium. There was a signal increase at 1000 nm as well as an increase in electron density value.
As it satisfies the 1000 nm McWhirter criterion, it is close to the McWhirter criterion in other coating thicknesses.

4.5. Calibration Studies

Samples of standard solutions of Pb, Cu, Cr with different concentrations were loaded in a volume of 500 nL on 75 nm, 300 nm, 450 nm and 1000 nm Si_3N_4 coated wafers. And, these wafers were left to dry at room temperature within 5 minutes. Afterwards, analyses were performed by 4 single laser pulses on the same droplet with 130 mJ energy. For statistical analysis, four seperate droplets for each concentrations were used.
Calibration graphs were obtained by plotting the relative signal strength of analytical line of interest against the analyte concentration. Detection limit values were obtained from the slope of the calibration curves. Figure 4.39, 4.40 and 4.41 show the calibration curves, line equations for chromium, copper and lead for each silicon nitride coating thicknesses of the substrates.

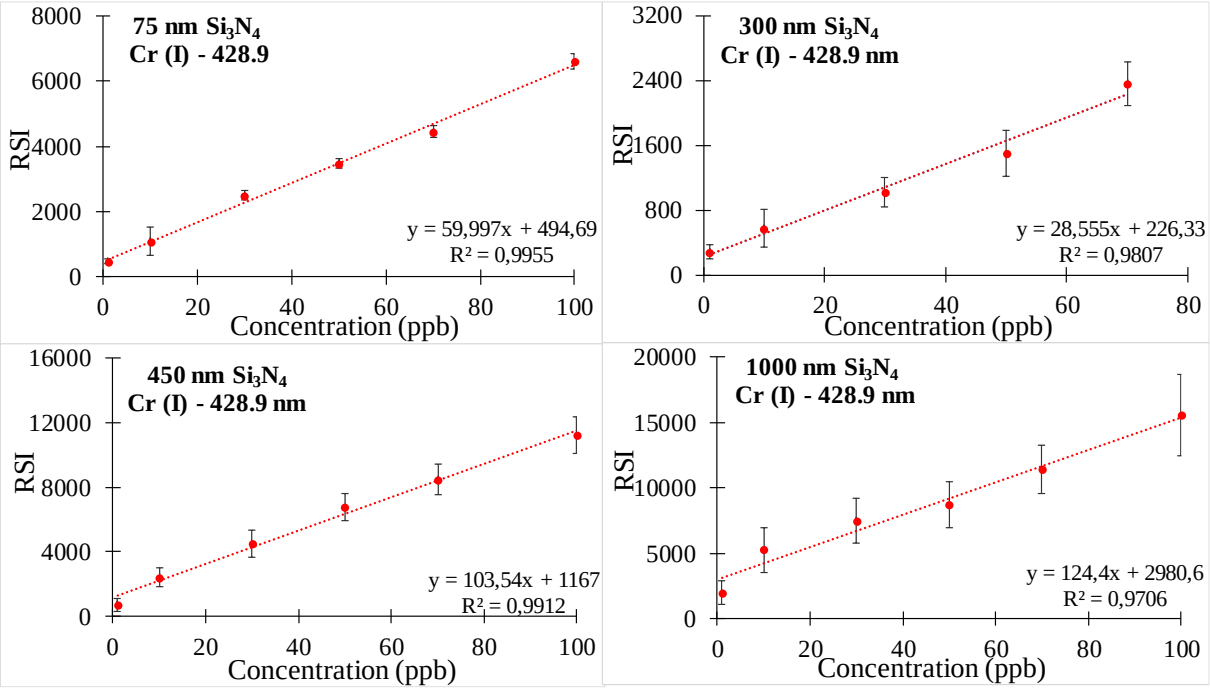

Figure 4.39. Cr (I) (428.9 nm) LIBS signal obtained from Cr solutions in the concentration range of 1ppb - 100 ppb on 75nm, 300nm, 450nm, 1000nm Si_3N_4 coated wafer layers.

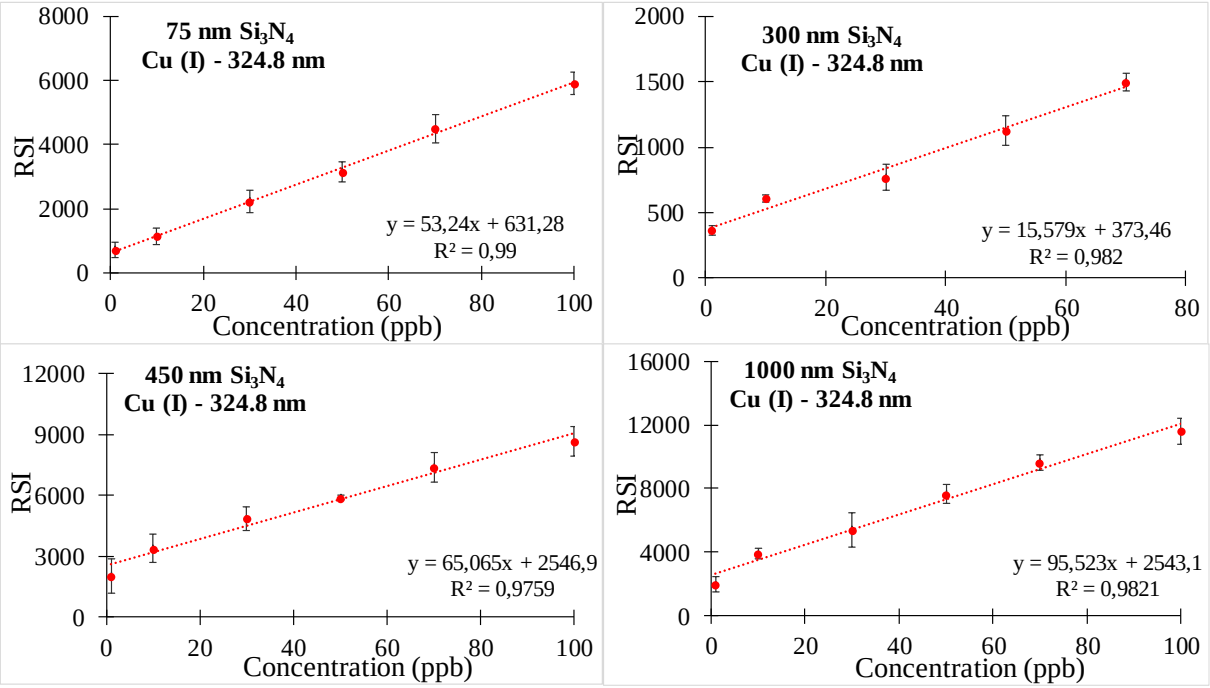

Figure 4.40. Cu (I) (324.7 nm) LIBS signal obtained from Cu solutions in the concentration range of 1ppb - 100 ppb on 75nm, 300nm, 450nm, 1000nm Si_3N_4 coated wafer layers.

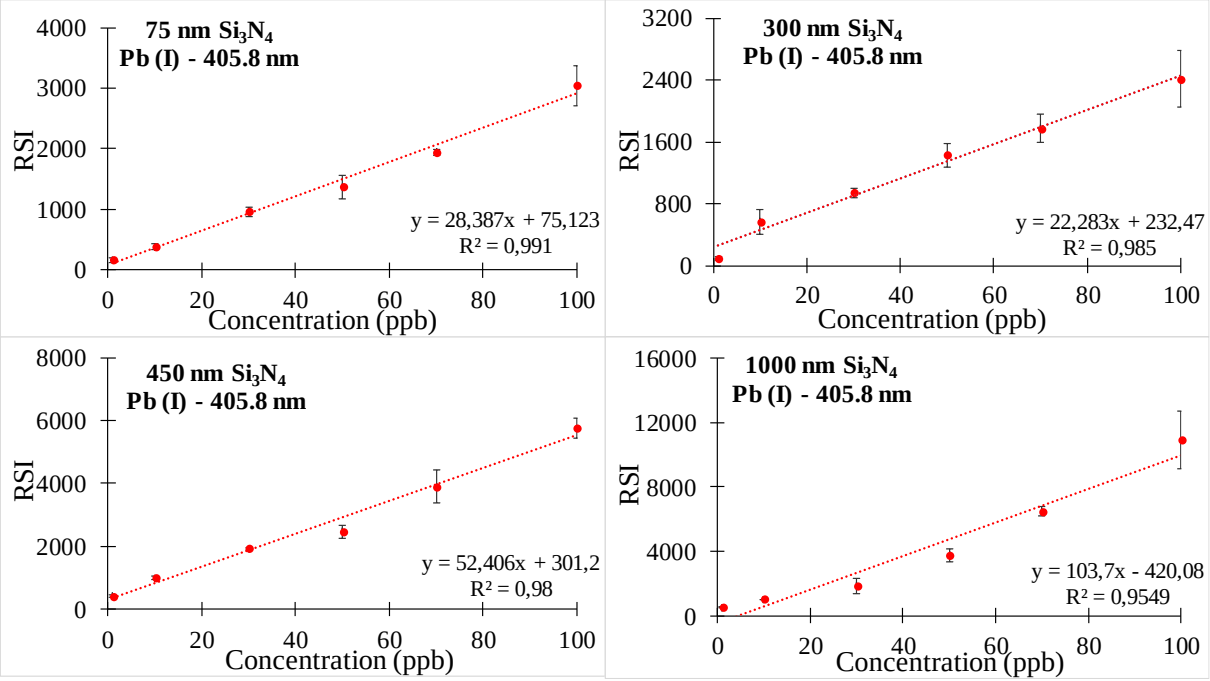

Figure 4.41. Pb (I) (405.8 nm) LIBS signal obtained from Pb solutions in the concentration range of 1ppb - 100 ppb on 75nm, 300nm, 450nm, 1000nm Si_3N_4 coated wafer layers.

Within the scope of this study, detection limits were calculated for each different thickness of each element. For this calculation, DL= $3SD_{(BG)}$ / slope equation was used. Detection limits calculated for each element with different coatings are given in Table 4.5, interms of both, in concentration unit and in absolute amounts.

Table 4.5. Detection limits obtained from the calibration curves of copper, chromium and lead elements on 75 nm, 300 nm, 450 nm and 1000 nm Si_3N_4 coated wafer by dry drop LIBS method.

	Limit of Detection (LOD)					
	Pb (I) - 405.8 nm		Cu (I) - 324.8 nm		Cr (I) – 428.9 nm	
Si_3N_4	pg	µg/L (ppb)	pg	µg/L (ppb)	pg	µg/L (ppb)
75 nm	1.64	3.27 +/-0,94	0,74	1.42+/- ,37	0.70	1.39 +/- 0,4
450 nm	0.97	1.93 +/- 0,20	0,44	0.88+/-0,25	0,64	1.29 +/- 0,2
1000 nm	0.7	1.39+/- 0,22	0,42	0.85 +/- 0,3	0,56	1.12 +/- 0,3
Aras 2019	11	22	0.5	1	1.5	3

The LOD improves from the 75 nm coated layer to the 1000 nm coated layer. In thicker nitride layers, the signal intensities increased and LOD values decreased. The results are given by taking the average over 4 separate droplets for each element and concentration studied.

Table 4.6. Some detection limits from the literature for chromium, copper and lead by LIBS

	LOD		
	Pb	Cu	Cr
Chen Z. et al., 2008	0.074 ppm	0.029 ppm	0.034 ppm
Lee Y. et al., 2012	75 ppb	0.64 ppm	18 ppb
Aras N. et al., 2012	13.6 ppb	1.99 ppb	6.49 ppb
DeGiacomo A. et al., 2015	0.2 pg	-	-
Martínez-Minchero M. et al., 2021	-	1150 ppm	-
Bol'shakov A. et al., 2021	300 ppb	10 ppb	-
Khan Z. H. et al., 2020	0.5 ppm	-	-
Salloom H. et al., 2021	51 ppb	41 ppb	40 ppb
This study (1000 nm Si_3N_4)	*1.4 ppb(0.7 pg)*	*0.85 ppb (0.4 pg)*	*1.12 ppb (0.6pg)*

In LIBS spectra of Chromium, the signal from Cr element was less noisy and the peaks were better defined. Therefore, the minimum concentration used in the calibration curve of Cr was extended to even smaller concentrations. It was observed that even lower concentrations than the estimated detection limit can be seen with a 1000 nm coated wafer for element of Cr. This point, extremely low concentrations range, needs to be studied in more detail.

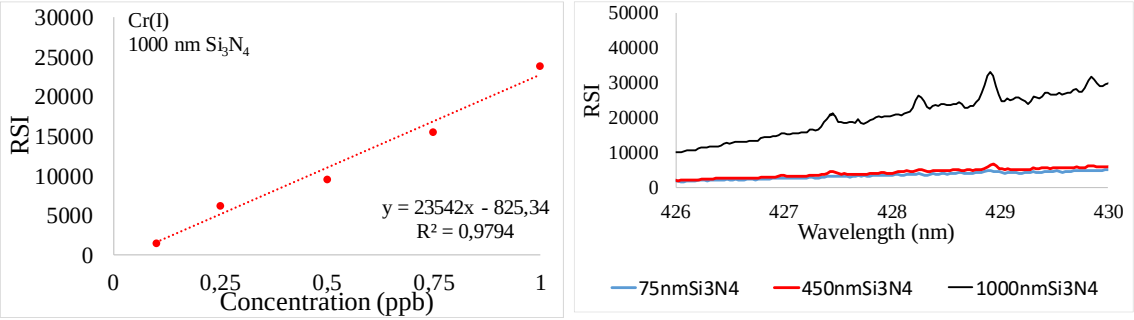

Figure 4.42. 0.25 ppb Cr calibration curve with 1000 nm coated Si_3N_4, LIBS spectra for 0.25 ppb Cr with 75 nm, 450 nm and 1000 nm Si_3N_4 coated wafers. In this way, invisible peaks are revealed and a good qualitative analysis is provided with 1000 nm.

The LOD results of this study is compared with the literature values obtained by LIBS but with different approaches. The amounts that could be detected in this study is drastically lower than competitive techniques. Especially, DeGiacomo's group result for Pb, which is nanoparticle enhanced LIBS study, and reports 2 pg Pb detection. In this study 0.7 pg Pb detection is achieved.

Signal / noise ratios for 10 ppb concentration are given in Table 4.7. Signal intensities increase in studies with very low concentrations of 1000 nm silicon nitride coating.

Table 4.7. Signal / noise ratios with 10 ppb concentration of heavy metal elements

Si_3N_4 Thickness	Pb – S/N	Cu – S/N	Cr – S/N
75 nm	6.2	38.2	19.1
450 nm	10.9	56	20.8
1000 nm	14.6	56	30

Signal: maximum peak height – average of the background

Noise: standard deviation of the background*2

4.6. Analytical Performance of the substrates

The analytical performance of the silicon nitride coated si-wafer substrates were tested by using certified reference samples, multielement standards and real water samples. According to the results observed; 1000 nm silicon nitride coated wafers

improves the LIBS signal intensity in the best way. Therefore, method validation and performance characteristics of the substrates were studied with using 1000 nm nitride coated wafers.

4.6.1. Certified Reference Materials, CRM, and Real Waters Analysis

In order to evaluate the accuracy and precision of the nitride coated substrate for dry-droplet analysis by LIBS, Certified Reference Water sample, DWS, European Reference Materials (ERM) and Multi Element Standard, ICP-PES solutions were used. The LIBS spectrum of the certified reference samples, DWS, ERM and ICP-PES, are given in Figures 4.43, 4.44 and 4.45, respectively. In each, relevant spectral regions

specific to the elements present are shown, enlarged.

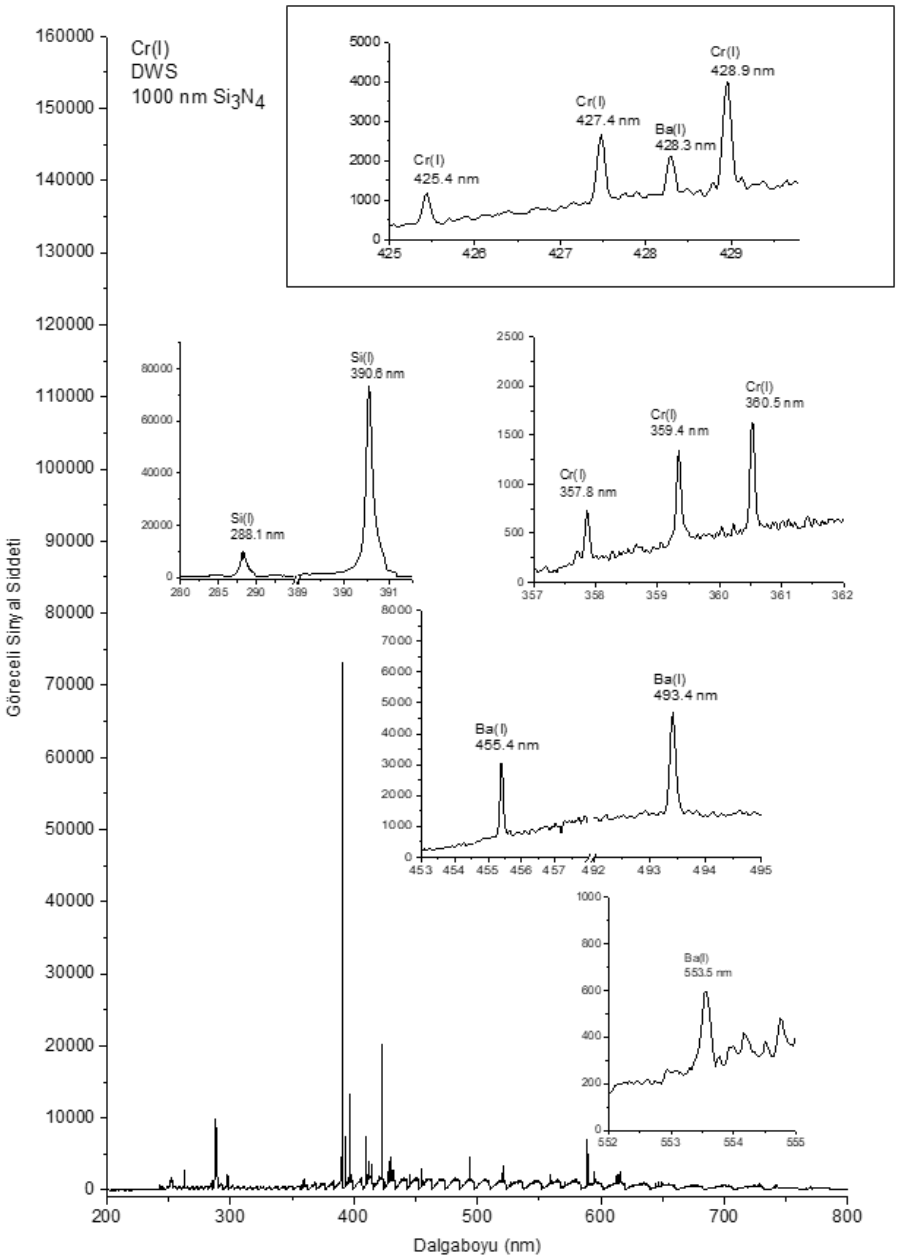

Figure 4.43. LIBS analysis of DWS solution under the conditions optimized for Cr - Sample is diluted to contain 30ppb Cr.

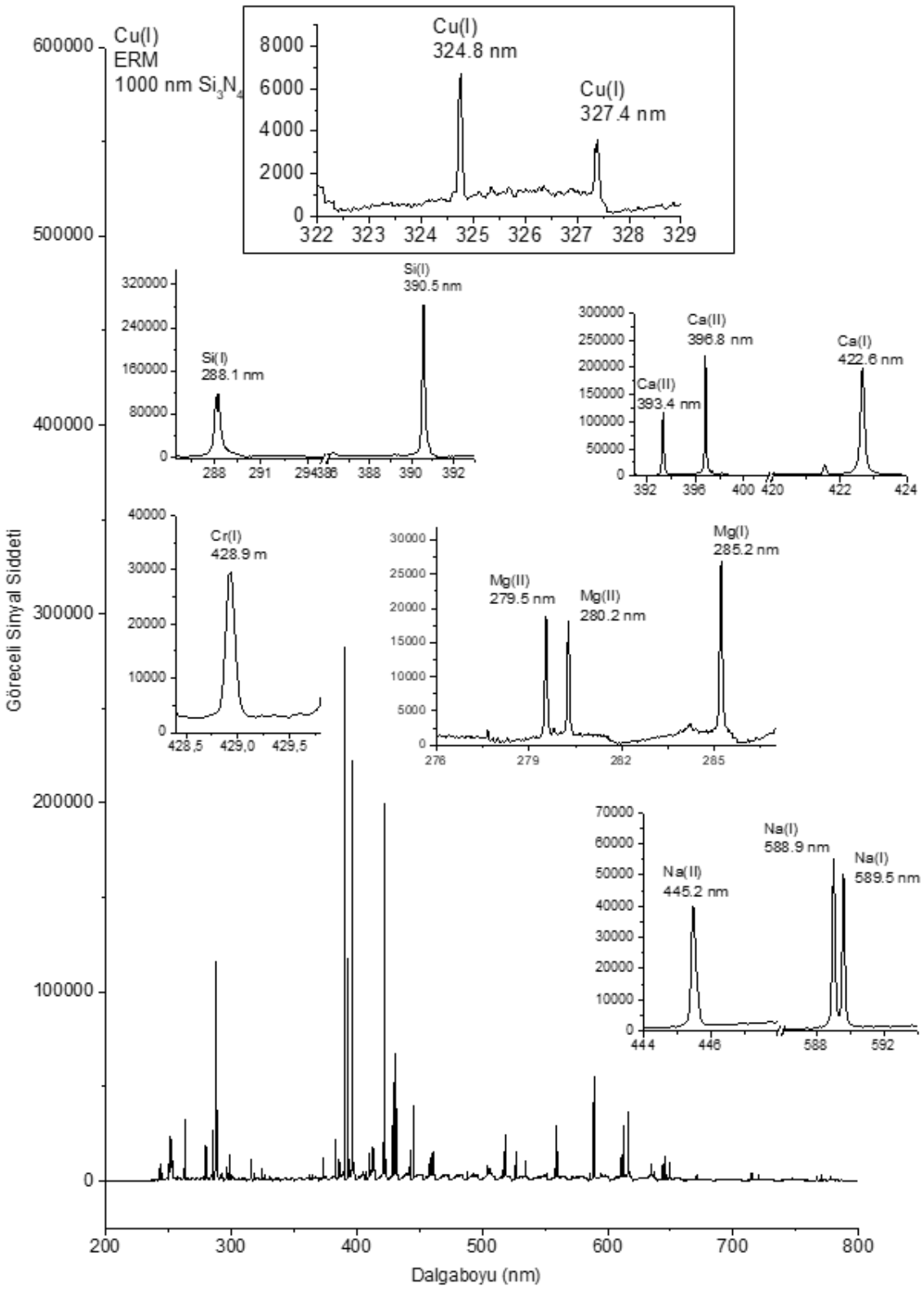

Figure 4.44. LIBS analysis of ERM solution under the conditions optimized for Cu - Sample is diluted to contain 50ppb Cu.

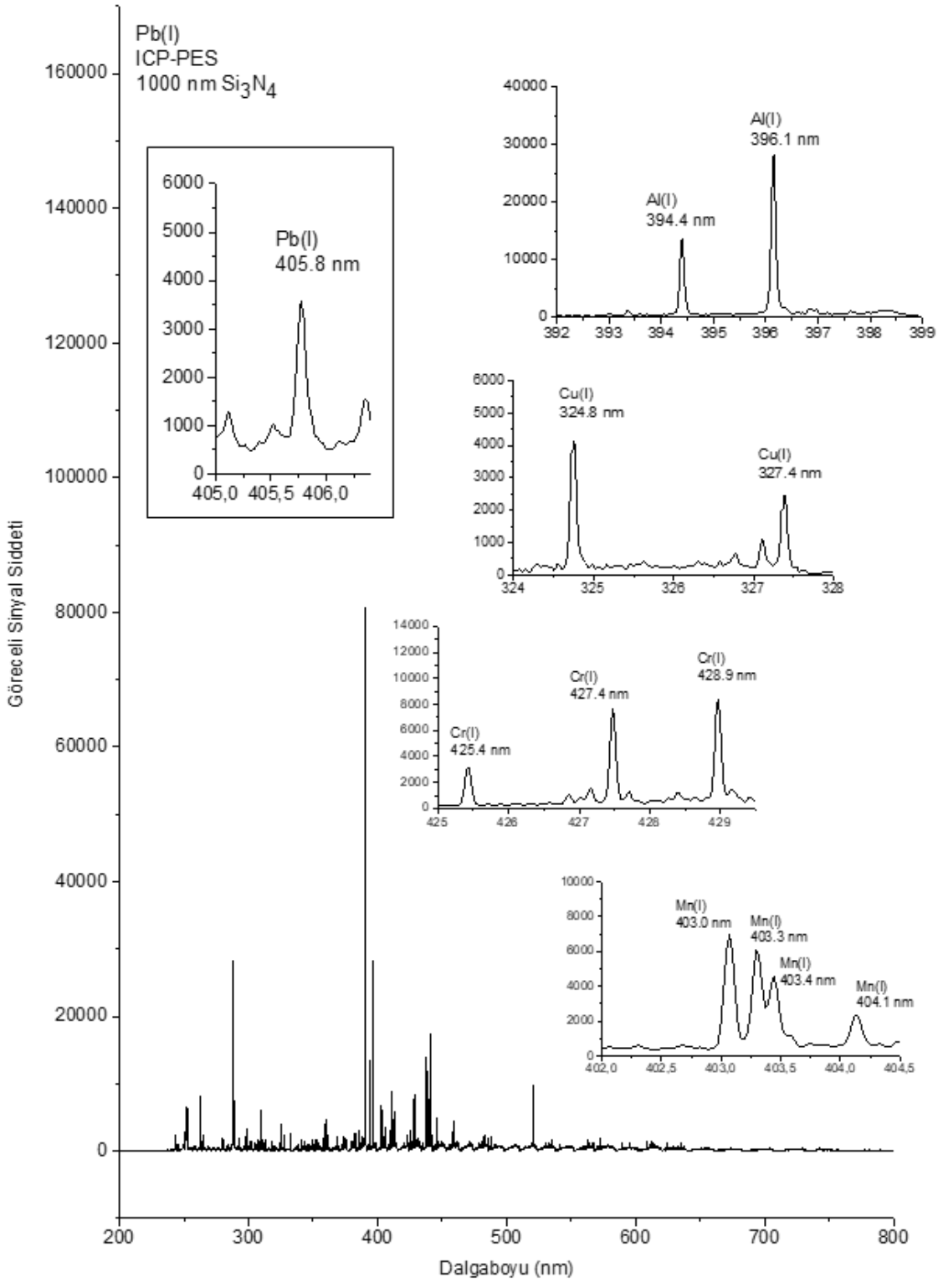

Figure 4.45. LIBS analysis of ICP-PES solution under the conditions optimized for Lead - Sample diluted to 50ppb Pb.

Some analytical figures of merit, like accuracy and precision were determined from CRM samples. The accuracy and precision The accuracy is defined as the closeness

of the analysis results to the true (certified) value and given as percent error. The precision is the agreement among individual analysis results of multiple measurements and usually expressed in terms of relative standard deviation of the measurements. Table 4.8 below, lists these performance characteristics calculated from the measurements made by using 1000 nm thick nitride coating. In terms of accuracy, 6, 21 and 19 % error were calculated for Cr, Cu and Pb, respectively. These values could be considered within the normal error range, especially for multielement standard samples where strong matrix effects are present.

Table 4.8. Performance characteristics of 1000 nm nitride coated wafer for dry-droplet LIBS analysis.

	Standard Solution	Multielement Solution	Percent Error Calculation (%)
LIBS SI for Cr(I) – 428.9 nm	8810,972	9586,867(***)	8
Cr(I) Concentration calculation using equation from calibration graph	50 ppb	53,1 ppb(***)	6
LIBS SI for Cu(I) – 324.8 nm	7327,337	6185,614(**)	18
Cu(I) Concentration calculation using equation from calibration graph	50 ppb	39,01 ppb(**)	21
LIBS SI for Pb(I) – 405.8 nm	3762,306	3266,872(*)	13
Pb(I) Concentration calculation using equation from calibration graph	50 ppb	40.193 ppb(*)	19

(*) - ICP-PES Trace Metal Solution (containing 50 ppb Pb)

(**) - ERM Hard Drinking Material– CRM LGC6026 (containing 50 ppb Cu)

(***) - Drinking Water Metal Solution – DWPS-A-100 (containing 50 ppb Cr)

Same experiments were performed on 300 nm silicon nitride coated wafer substrate for comparison purposes and the results are shown in Figure 4.46, graphically.

Relative signal intensity of the elements enhances for more than an order of magnitude from 300 nm nitride coated substrates to 1000 nm coated ones.

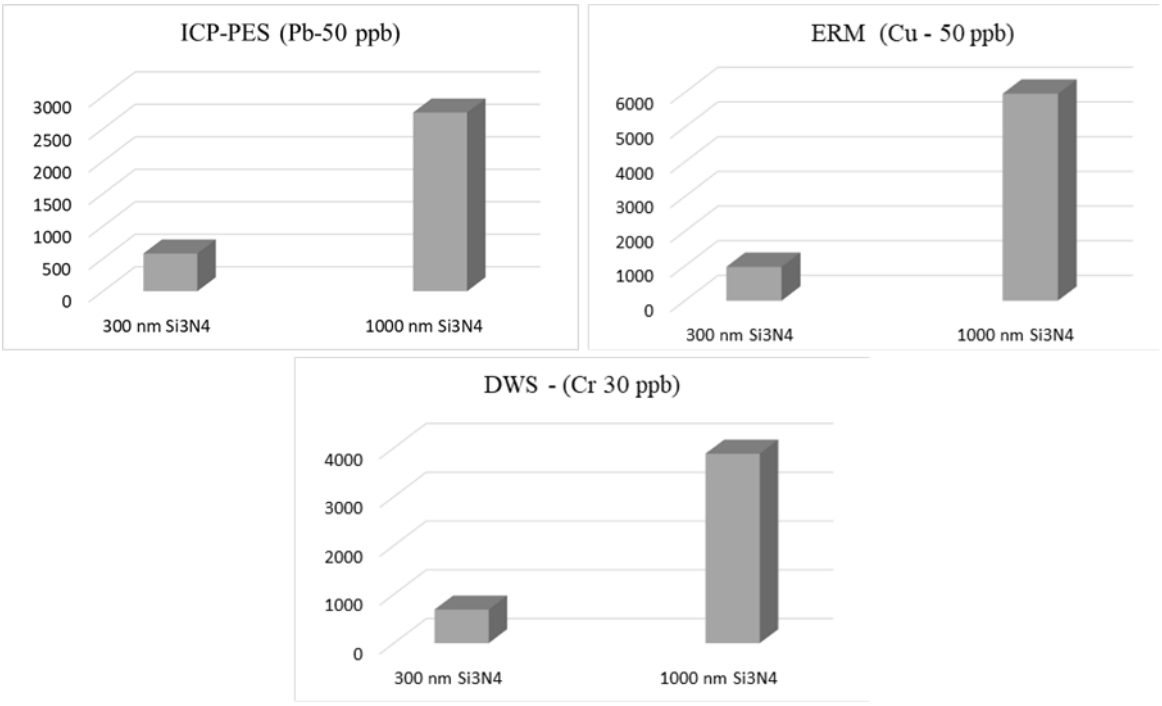

Figure 4.46. Relative signal intensity of the elements Pb, Cu and Cr on 300 nm and 1000 nm Si_3N_4 coated wafers for ICP-PES, ERM and DWS water samples.

4.6.2 Recovery studies from spiking experiments

For the determination of the percent recovery values for dry-droplet LIBS analysis based on the use of nitride coated substrates, two different real water samples were spiked with Cr, Pb and Cu standard solutions, separately. For this purpose, some portions of heavy matrix containing real water sample, SLRS-4 River Water, with undetectable Cr concentration, were spiked with differing concentrations of Cr standard solutions. On the other hand, real drinking water sample, OZSU, bought from a local market were spiked with Pb and Cu standards. Figure 4.47 shows the spectral region for Cr lines, from the LIBS analysis of SLRS-4 river water sample. No chromium lines detected in this sample however, relatively high concentrations of 22 elements are present. Therefore, Cr with different concentrations are spiked in this sample.

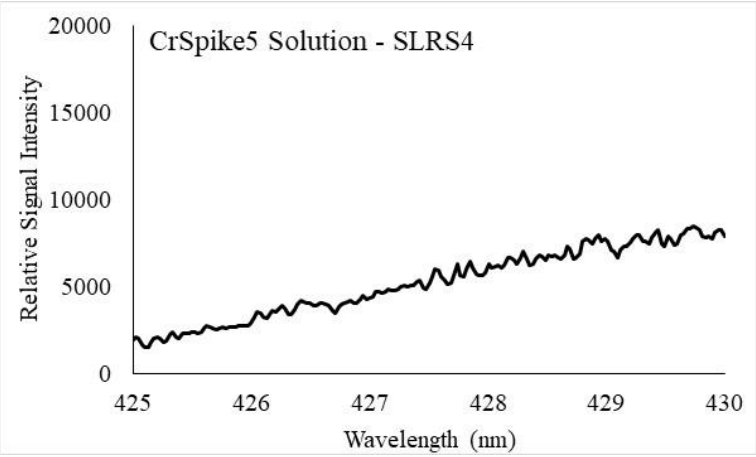

Figure 4.47. A region of the LIBS spectrum from the analysis of SLRS-4 river water sample

Calibration graphs drawn for LIBS analysis of four Cr spiked solutions is shown in Figure 4.48, and a linear relationship between concentration and emission strength is observed.

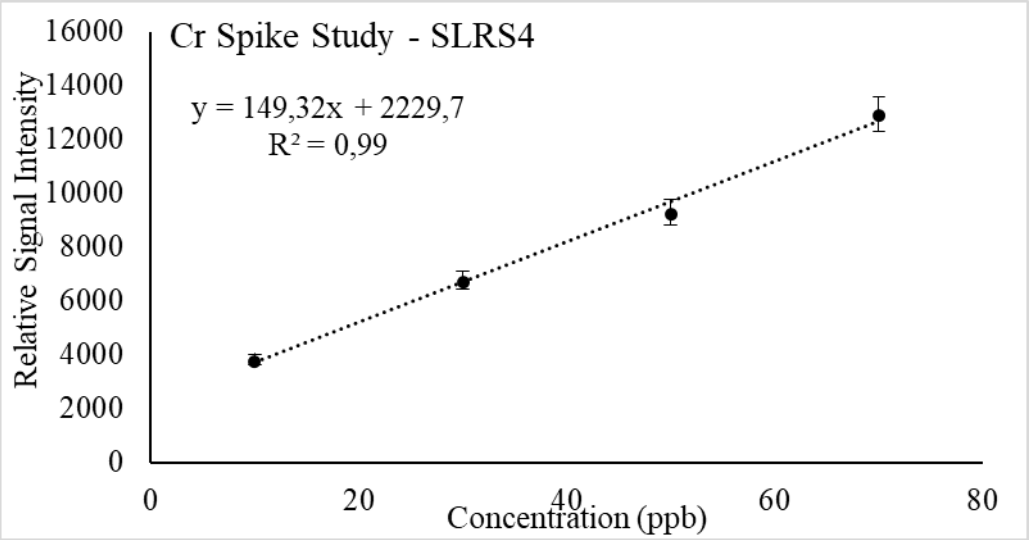

Figure 4.48. The calibration graph for 70, 50, 30 and 10 ppb Cr spiked river water samples.

The LIBS signal strengths observed for Cr spiked river water solutions were extrapolated to concentration axis on the calibration graph drawn for standard Cr solutions, then the recovery values were calculated from the estimated concentrations. Table 4.9 lists the recoveries obtained from spiking experiments. In cases with high analyte (30, 50, 70 ppb Cr), and low matrix concentrations, the percent recovery values

are higher. Whereas, as low as 67.8 % recovery value was obtained from a solution with high matrix concentrations.

Table 4.9. Percent Recovery values obtained from Cr Spiking study

Spike Name	Concentration (ppb)	Concentration from the eqn.	Recovery (%)
CrSpike1	70	80,22	114,5
CrSpike2	50	50,96	102,0
CrSpike3	30	30,5	101,6
CrSpike4	10	6,78	67,8

For the Pb spiking study, same amounts of drinking water from a local market were spiked with 70, 50, 30 and 15 ppb Pb standard solutions. Figure 4.49 shows the spectral region for Pb(I) lines at 405.8 nm, from the LIBS analysis of unspiked OZSU water sample.

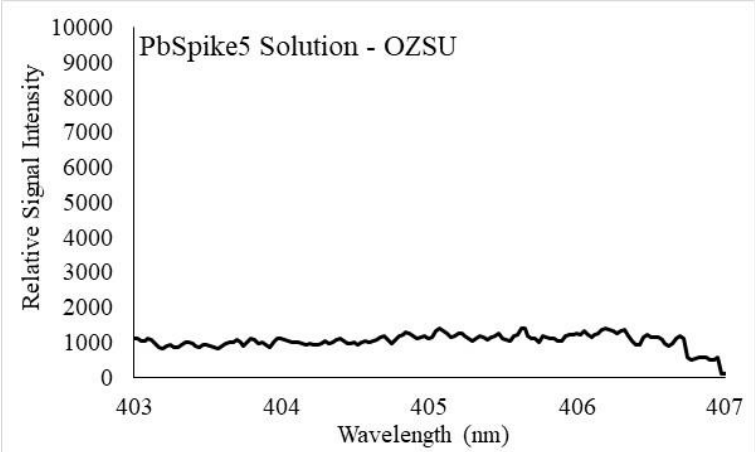

Figure 4.49. A region of the LIBS spectrum from the analysis of OZSU water sample

Figure 4.50 shows the calibration curve of for Pb spiked solutions.

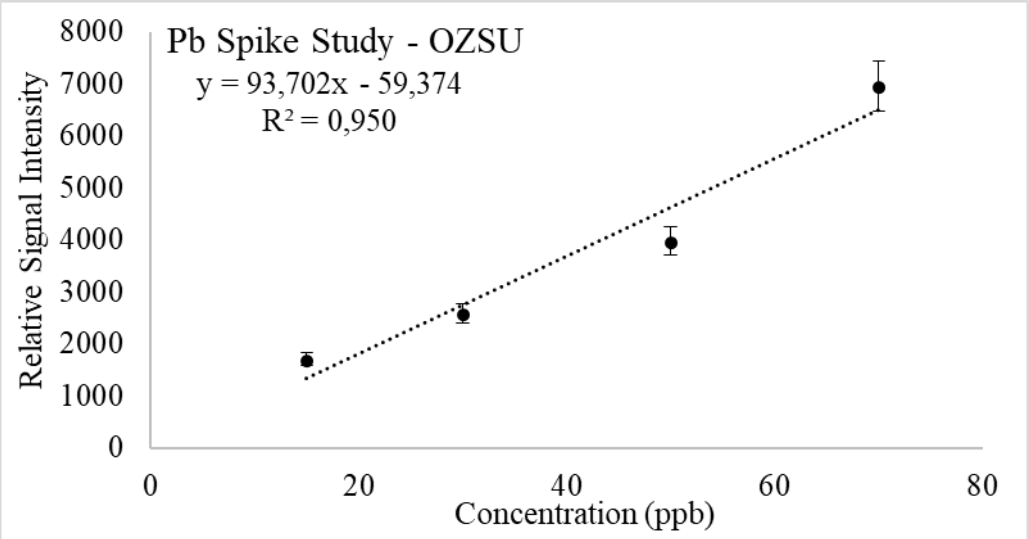

Figure 4.50. The calibration graph for 70, 50, 30 and 15 ppb Pb spiked OZSU water samples

Calculations were made over the equation of the calibration graph obtained from the standard Pb solutions and recovery values calculated are given in Table 4.10.

Table 4.10. Percent Recovery values obtained from Pb spiking study

Spike Name	Concentration (ppb)	Concentration from the eqn.	Recovery (%)
PbSpike1	70	71,13	101,7
PbSpike2	50	42,42	84,8
PbSpike3	30	28,0	93,3
PbSpike4	15	20,49	136,6

For the Cu spiking study, same amounts of drinking water from a local market were spiked with 70, 50, 30 and 10 ppb Cu standard solutions. Figure 4.51 shows the spectral region for Cu(I) lines at 324.7 nm, from the LIBS analysis of unspiked OZSU water sample.

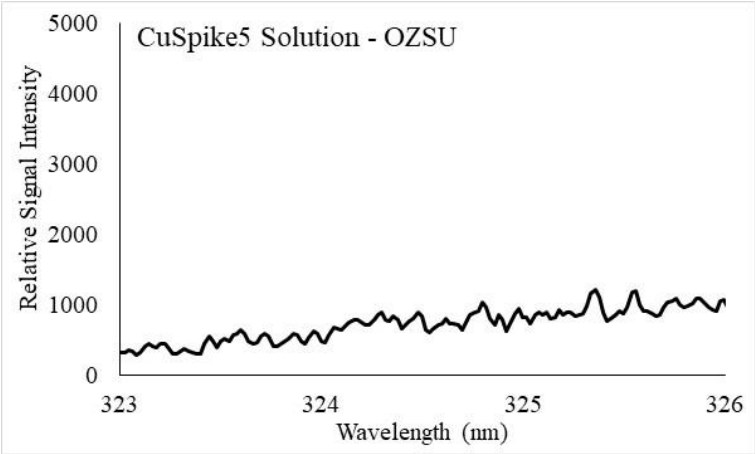

Figure 4.51. A region of the LIBS spectrum for Cu, from the analysis of OZSU water sample

Figure 4.52 shows the calibration curve of for Cu spiked solutions.

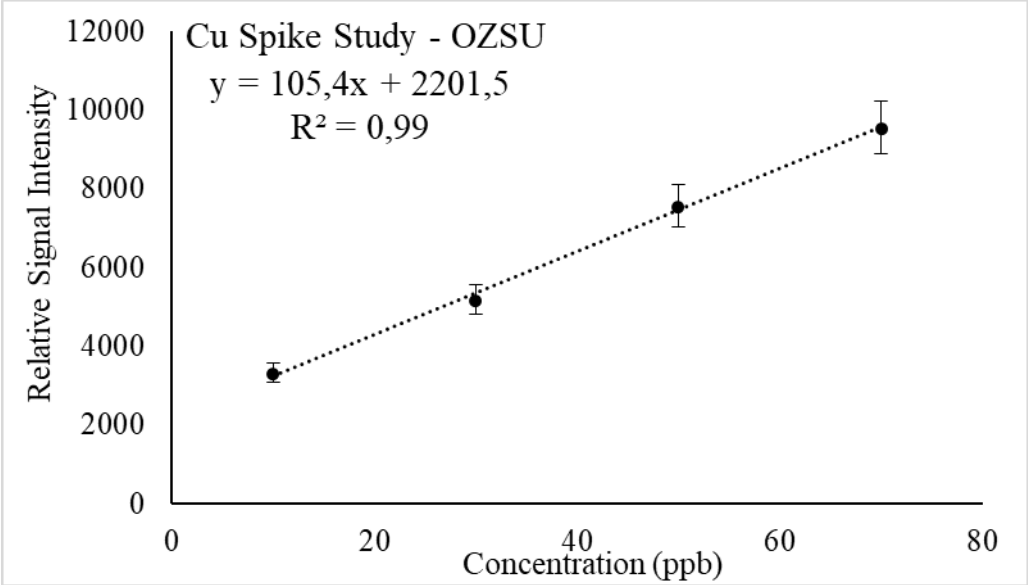

Figure 4.52. The calibration graph for 70, 50, 30 and 10 ppb Cu spiked OZSU water samples

Using the LIBS signal intensities obtained, calculations were made over the equation of the calibration graph constructed with standard Pb solutions. Percent recovery values are listed in Table 4.11.

Table 4.11. Percent Recovery values obtained from Cu spiking study

Spike Name	Concentration (ppb)	Concentration from the eqn.	Recovery (%)
CuSpike1	70	73,6	106,2
CuSpike2	50	52,63	105,3
CuSpike3	30	27,07	90,2
CuSpike4	10	8,3	83

As is observed in Cr and Pb cases, the higher recoveries are obtained with high concentration spiking samples whereas lower recovery is obtained for low concentration sample

CHAPTER 5

CONCLUSION

Within the scope of this study, the effect of silicon nitride coating thickness on LIBS signal strength of some heavy metals (Pb, Cu, Cr) in aqueous environments has been investigated.

For this purpose, silicon wafers coated with thicknesses of 75 nm, 300 nm, 450 nm and 1000 nm Si_3N_4 layers were comparatively studied as target substrate. Based on the use of dry-droplet LIBS method, a liquid to solid conversion strategy, 500 nL volume of liquid droplets were loaded onto the substrates, dried at room temperature and analyzed afterwards by LIBS.

Experimental LIBS parameters, detector delay time, gate time and laser pulse energy were optimized. Under the optimum conditions, calibration curves constructed, analytical figures of merit determined.

Among the four different thicknesses of silicon nitride coatings, 1000 nm nitride coated layer substrates have provided the highest signal enhancement compared to 300 nm coated one for all the elements studied. Compared to the 300 nm nitride coated layer; 75 nm nitride coated layer exhibited 1.26 to 2.29 fold increase in LIBS signal, whereas the 450 nm nitride coated layer increases the LIBS signal between 2.18 and 3.35 times. For 1000 nm nitride coated layer, between 3.0 to 4.52 fold enhancement in LIBS signal was observed and the rate of increase is element dependent.

When comparing the results of 300 nm Si_3N_4 coatings studied in our group previously and the results of the 75 nm Si_3N_4 coatings, an overall increase in the signal levels observed. This increase can be interpreted as anti-reflective behaviour of thin film coatings when the coating thickness is smaller than the wavelength of radiation that interacts with the surface.
For optimum coating thickness calculation. The formula $d = \lambda_0 / 4n$ is used.

d: optimum coating thickness (um),

λ: used light wavelength (um),

n: the 'silicon nitride' refractive index of the material used.

For the 532 nm laser light, and when the value of 2.05, which is the refractive index of silicon nitride at that wavelength, is replaced in the formula, the result shows that the coating value of 0.065 μm is the optimum coating thickness. In this study, 75 nm nitride coated layers with the closest one to 65 nm thickness were available commercially and were used as the thinnest nitride coated layer. The theoretical reflectance values were also confirmed through UV-Vis reflectance spectral measurements, given in Figure 4.27.

As a result of these measurements, Si_3N_4 coating thickness with 75 nm thickness gave the lowest reflectance value as calculated in theory. The reason why 75 nm coating increases the signal intensity slightly compared to 300 nm coating can be considered to reflect less laser light and use more for absorption

Then, as the thickness of the 450 nm and 1000 nm nitride coated layer increases, the signal intensity increases linearly, mainly due to the increase in nitride presence. The classification resulting from the thickness of the silicon nitride coating is divided into thin film coating and thick film coating. Anti-reflective effects from thin film coatings occur when the coating thickness is thinner than light that interacts with the surface. Thick film coating effect occurs at thicknesses greater than the wavelength of the light studied. Considering that the laser source we use provides 532 nm light, it is thought that the 1000 nm thick coating layer will show the thick film effect. In LIBS signal results, it was clearly seen that the results of the analysis performed by loading heavy metals on the 1000 nm Si_3N_4 coating with the dried droplet method enable qualitative and quantitative analysis by amplifying even very low signals. The physical properties and specific thermal properties of silicon nitride play a major role. Measurements were taken with a profilometer with the need to investigate *absorption and optical penetration depth*. The depth of the laser pulses was measured with a profilometer in order to understand how deep the surface was penetrated and to observe the bulk silicon effect by making 4 consecutive single laser pulses on the dried droplet with LIBS. With this study, it was seen that there was an average depth of 0.750 micrometers. However, due to the Gaussian feature of the laser beam used, the etching is similar to the "V" shape and the laser pulses can go beyond the nitride coating and interact with the lower silicon layer. However, it can be said that it interacts less with bulk silicon as you go towards 1000 nm thickness.

In this respect, the reason why the signal intensities are observed to be consistently high in 1000 nm coated layers can be seen as the laser energy is caused by the interaction of only the nitride layer and the low effect of the substrate silicon. The same LIBS studies can be carried out with pure nitride layers without silicon substrate. However, it can cause an economic disadvantage. In addition, too much signal amplification of 1000 nm coating causes the background values to fluctuate too high, thus increasing the standard deviations.

Besides these issues, the thermal conductivity is also a factor for our discussions. Thermal conductivity expressed in the form of $k = \frac{Q}{t} * \frac{L}{A.\Delta T}$, as can be seen, depends on the amount of heat (Q), time (t), surface area of heat transfer (A), material thickness (L), and temperature difference (T) that causes heat transfer.

In the experimental setup we use, assuming that for each of the four different coatings (75nm, 300nm, 450nm, 1000 nm Si_3N_4), the amount of heat, Q, the surface area of the heat transfer, A, time, t and the temperature difference, ΔT are the same, that is, we can say that there is a linear relationship between the thickness of the silicon nitride used and the thermal conductivity. In other words, as the thickness increases, the thermal conductivity increases. High thermal conductivity is mainly based on 2 main issues as; electronic effect and lattice vibration. The electronic effect plays a role in metals. High thermal conductivity is observed in non-metallic materials due to lattice vibration. Lattice effect arises from the sequence of molecules in the substance. For example, amorphous materials such as wood provide low conductivity, but when we look at diamond, we can see its high thermal conductivity due to the lattice arrangement (Thermal Conductivity and Diffusivity, 2017). Due to this lattice vibration in thicker silicon nitride coatings the silicon nitride material behaves like metal materials. In this way, it has been observed that the LIBS signal intensity is increased with metal substrates in the literature, and the LIBS signal intensity is significantly improved in thick silicon nitride coatings, just like the effect of metal substrates. With metal substrates, there were negative effects such as the fact that the aqueous droplets did not spread homogeneously or the signal decrease observed due to the metal surfaces creating too much pollution in the spectrum, but with this thick silicon nitride coating, these negative effects were not observed and signal improvement was observed like a metal substrate.

The increase in plasma temperature and electron density from low thickness coatings to high thickness is one of the evidences of LIBS signal increase. In this respect, the LOD values shown by theoretical calculations increased less than desired. The detection limits of 1000 nm nitride coated layer are 0.7 pg for lead, 0.42 pg for copper and 0.56 pg for chromium. With our studies, it is seen that the method can also be applied to the reference waters multi-element analysis.

With this method, most heavy metals can be detected at lower concentrations compared to other methods applied for liquids analysis by LIBS. With the technique used, it can be detected even if they are present in amounts below the heavy metal limits in the drinking water standards of organizations such as EPA and WHO.

REFERENCES

Aguirre M., Legnaioli S., Almod'ovar F., Hidalgo M., Palleschi V., Canals A. 2013. Elemental analysis by surface-enhanced Laser-Induced Breakdown Spectroscopy combined with liquid–liquid microextraction . Spectrochim. Acta B: 79 ,88–93.

Alamelu D., Sarkar A., Aggarwal S., 2008. Laser-İnduced Breakdown Spectroscopy For Simultaneous Determination Of Sm, Eu And Gd İn Aqueous Solution. Talanta.77 :256– 261.

Aras N. , Ünal S., Arıca D. , Yalçın Ş., 2012. Ultrasonic nebulization-sample introduction system for quantitative analysis of liquid samples by laser-induced breakdown spectroscopy. Spectrochimica Acta Part B: Atomic Spectroscopy. 74-75, 87-94.

Aras N., Yalçın S. 2016. Development and validation of a laser-induced breakdown spectroscopic method for ultra-trace determination of Cu, Mn, Cd and Pb metals in aqueous droplets after drying, Talanta 149.53–61.

Aras N., Yalçın Ş.. 2018. Investigating silicon wafer based substrates for dried-droplet analysis by Laser-Induced Breakdown Spectroscopy. Spectrochimica Acta Part B: 152: 84–92

Bae D., Nam S., Han S., Yoo J., Lee Y., 2015. Spreading A Water Droplet On The Laser- Patterned Silicon Wafer Substrate For Surface-Enhanced Laser-İnduced Breakdown Spectroscopy, Spectrochimica Acta Part B: Atomic Spectroscopy. 113, 70–78.

Brown Matthew S. and Arnold Craig B. 2010. Fundamentals of Laser-Material Interaction and Application to Multiscale Surface Modification. Springer Series in Materials Science 135, DOI 10.1007/978-3-642-10523-4

Caceres J.O., López J.T., Telle H.H., Ureña A.G. 2001. Quantitative analysis of trace metal ions in ice using laser-induced breakdown spectroscopy, Spectrochim.Acta B 56 (6). 831–834.

Cahoon E. M., Almirall J.R., 2012. 'Quantitative Analysis of Liquids from Aerosols and Microdrops Using Laser Induced Breakdown Spectroscopy. Anal. Chem. 84(5) : 2239-2244.

Charge-coupled device, Wikipedia, The Free Encyclopedia

Chen Z., Li H., Liu M., Li R. 2008. Fast And Sensitive Trace Metal Analysis İn Aqueous Solutions By Laser-İnduced Breakdown Spectroscopy Using Wood Slice Substrates. Spectrochim. Acta B: 63: 64–68.

Cremers, D. A., and Radziemski. 2006. Handbook of Laser-Induced Breakdown Spectroscopy. England :John Wiley& Sons. Inc.

Critchley L. 2018. How to Measure the Success of Antireflective Coatings, Azo Materials, https://www.azom.com/article.aspx?ArticleID=15807

Colbeck, I.,, Lazaridis M. 2014. Aerosol Science: Technology and Applications. John Wiley & Sons - Science. ISBN 978-1-119-97792-6.).

Dayan, A. D. and Paine, A. J. (2001). Mechanisms of chromium toxicity, carcinogenicity and allergenicity: Review of the literature from 1985 to 2000. Human and Experimental Toxicology 20 (9): 439-451.

De Giacomo A., Gaudiuso R., Koral C., Dell'Aglio M., De Pascale O. 2013. Nanoparticle-Enhanced Laser-Induced Breakdown Spectroscopy of Metallic Samples. Anal. Chem. 85: 10180−10187

Filho E. R. P., Sperança M. A., Andrade D.F. 2017. Different sample preparation methods for analysis of suspension fertilizers combining LIBS and liquid-to-solid matrix conversion: determination of essential and toxic elements. Analytical Methods 9(35). DOI:10.1039/C7AY01049D.

Griem, H. R. 1964. Plasma Spectroscopy. New York: McGraw-Hill Book Company

Hahn D. W., Lunden M. M. 2000. Detection and Analysis of Aerosol Particles by Laser-Induced Breakdown Spectroscopy, Aerosol Science & Technology, 33:1-2, 30-48, DOI: 10.1080/027868200410831

Hainaut, Oliver R. December 2006. "Basic CCD image processing". Retrieved January 15, 2011

Hidalgo M., Aguirre M. A.,Nikolova H., and Canals A.. 2015. Hyphenation of single-drop microextraction with laser-induced breakdown spectrometry for trace analysis in liquid samples: a viability study. Analytical Methods, 3.

Huang J. , Ke C., Lin C. 2004. Matrix Effect On Emission/Current Correlated Analysis In Laser-İnduced Breakdown Spectroscopy Of Liquid Droplets. Spectrochimica Acta Part B: 59(3) : 321-326.

Järup L. 2003. Hazards of heavy metal contamination. Br Med Bull. 68(1):167–182.

Lambert M, Leven BA, Green RM. 2000. New methods of cleaning up heavy metal in soils and water; Environmental science and technology briefs for citizens; Manhattan, KS: Kansas State University.

Lazic V. and Ciaffi M. 2017. Laser-Induced Breakdown Spectroscopy Applied on Liquid Films: Effects of the Sample Thickness and the Laser Energy on the Signal Intensity and Stability. Journal of Spectroscopy,1-10. DOI:10.1155/2017/7872504

Lee Y., Oh S.W., Han S.H., 2012. Laser-İnduced Breakdown Spectroscopy (LIBS) Of Heavy Metal İons At The Sub-Parts Per Million Level İn Water. Appl. Spectrosc. 66(12): 1385–1396.

Mathew, Blessy B. Jaishankar, Monisha, Tseten, Tenzin, Anbalagan, Naresh, and Beeregowda, Krishnamurthy N. 2014. "Toxicity, mechanism and health effects of some heavy metals" Interdisciplinary Toxicology, vol.7, no.2, 2014, pp.60-72. https://doi.org/10.2478/intox-2014-0009

Matsumoto A., Shimazu Y., Nakano H. Murakami K., Yae S. 2021. Signal stability of surface-enhanced laser-induced breakdown spectroscopy for microdroplet analysis using a porous silicon substrate

Mohanty M, Kumar Patra H. Effect of ionic and chelate assisted hexavalent chromium on mung bean seedlings (Vigna Radiata l. Wilczek. Var k-851) during seedling growth. JSPB. 2013;9(2):232–241.

Nagajyoti, P.C., Lee, K.D., Sreekanth T.V.M. 2010. Heavy metals, occurrence and toxicity for plants: a review. Environ Chem Lett 8, 199–216. doi.org/10.1007/s10311-010-0297-8

Niu S.,Zheng L., Khan A., Yuan S., Yu J., Zeng H. 2016. Comparative study of the matrix effect in Cl analysis with laser-induced breakdown spectroscopy in a pellet or in a dried solution layer on a metallic target. Spectrochimica Acta Part B: Atomic

Spectroscopy, 118, 66-71.

Radziemski L. J., Cremers D. A. 1989. Laser Induced Plasmas and Applications, Marcel Dekker, New York 21(22) : 295-326.

Ryklis E.A., Bolgar A.S., Fesenko V.V.. 1969. Evaporation and thermodynamic properties of silicon nitride, Powder Metall. Met. Ceram. 8 (1), 73–76.

Sarkar A., Aggarwal S.K., Sasibhusan K., Alamelu D. 2010. Determination of sub-ppm levels of boron in ground water samples by laser induced breakdown spectroscopy, Microchim. Acta 168 (1–2) 65–69.

Silicon Nitride. Wikipedia, The Free Encyclopedia. https://en.wikipedia.org/wiki/Silicon_nitride.

Simeonsson J. B., Williamson L.J. 2011. Characterization of laser induced breakdown plasmas used for measurements of arsenic, antimony and selenium hydrides. Spectrochimica Acta Part B Atomic Spectroscopy 66(9-10). DOI:10.1016/j.sab.2011.08.003

Sirven J.-B., Rollin E., Musset O., Legay G.,.Vercouter T. 2021. A standardized method for characterization of matrix effects in laser-induced breakdown spectroscopy. Spectrochim. Acta B 179

Thermal Conductivity and Diffusivity, 2017.Lucid Learning. https://medium.com/@lucidlearning314/thermal-conductivity-and diffusivity- e6d3b5ee7ce5.

Ünal S., Yalçın Ş. 2010. Development Of A Continuous Flow Hydride Generation Laser-İnduced Breakdown Spectroscopic System: Determination Of Tin İn Aqueous Environments. Spectrochimica Acta Part B: 65:750–757.

Yang X., Li x., Cui Z., Yao G., Zhou Z., Li K. 2020. Improving the Sensitivity of Surface-Enhanced Laser-Induced Breakdown Spectroscopy by Repeating Sample Preparation. Optics and Photonics.

Zhong S., Zheng R., Lu Y., Cheng K., Xiu J.. 2015. Ultrasonic Nebulizer Assisted LIBS: a Promising Metal Elements Detection Method for Aqueous Sample Analysis. Plasma Science and Technology 17(11):979-984. DOI:10.1088/1009-0630/17/11/17

Wafers, MicroChemicals.

https://www.microchemicals.com/products/wafers/wafers_sinx_si3n4_sio2.html

Zhu S., Lo G.Q., Kwong D.L.. 2013. Silicon nitride based plasmonic components for CMOS back-end-of-line integration, Opt. Express 21 (20), 23376–23390.